



# A Review of Recent Solar Type III Imaging Spectroscopy

Hamish A. S. Reid\*

Mullard Space Science Laboratory, Department of Space and Climate Physics, University College London, Dorking, United Kingdom

## OPEN ACCESS

### Edited by:

Nicole Vilmer,  
Centre National de la Recherche  
Scientifique (CNRS), France

### Reviewed by:

Rohit Sharma,  
University of Applied Sciences and  
Arts Northwestern Switzerland,  
Switzerland  
Pierre Henri,  
UMR7328 Laboratoire de physique et  
chimie de l'environnement et de  
l'Espace (LPC2E), France

### \*Correspondence:

Hamish A. S. Reid  
hamish.reid@ucl.ac.uk

### Specialty section:

This article was submitted to  
Stellar and Solar Physics,  
a section of the journal  
Frontiers in Astronomy and Space  
Sciences

**Received:** 14 April 2020

**Accepted:** 28 June 2020

**Published:** 24 September 2020

### Citation:

Reid HAS (2020) A Review of Recent  
Solar Type III Imaging Spectroscopy.  
*Front. Astron. Space Sci.* 7:56.  
doi: 10.3389/fspas.2020.00056

Solar type III radio bursts are the most common impulsive radio signatures from the Sun, stimulated by electron beams traveling through the solar corona and solar wind. Type III burst analysis provides us with a powerful remote sensing diagnostic tool for both the electron beams and the plasma they travel through. Advanced radio telescopes like the LOw Frequency ARray (LOFAR), the Murchison Widefield Array (MWA) and the Karl G. Jansky Very Large Array (VLA) are now giving us type III imaging spectroscopy with orders of magnitude better resolution than before. In this review, the recent observational progress provided by the new observations is discussed for type III bursts at GHz and MHz frequencies, including how this enhanced resolution has facilitated study of type III burst fine structure. The new results require more detailed theoretical understanding of how type III bursts are produced. Consequently, recent numerical work is discussed which improves our understanding of how electron beams, Langmuir waves and radio waves evolve through the turbulent solar system plasma. Looking toward the future, some theoretical challenges are discussed that we need to overcome on our quest to understand type III bursts and the electron beams that drive them.

**Keywords:** solar flares, electron transport, electron acceleration, solar corona, solar type III bursts, beam plasma instabilities

## 1. INTRODUCTION

Type III radio bursts are the most common coherent radio emission produced by the Sun. Type III bursts are an indirect signature of energetic electrons propagating through the plasma of the solar corona and the solar wind. A gift of non-linear physics, the more we understand type III bursts, the more we can use them as remote sensing tools for astrophysical plasma. As high energy electron beams propagate through plasma with decreasing background electron densities, and hence decreasing plasma frequency, they emit type III radio emission at correspondingly decreasing radio frequencies. The spatial and spectral evolution of type IIIs thus contains a wealth of plasma dynamics information that has been studied for many decades since their first observational report by Payne-Scott et al. (1947). Analysis of type IIIs can provide insight on astrophysical processes including particle acceleration, charged particle transport through plasma, and the structure of solar system plasma. Space-based observations can detect *in situ* the electron beams, their associated plasma waves and radio spectra. However, we are dependent upon Earth-based telescopes to provide type III imaging, which we obtain above the 10 MHz ionospheric cut-off. These frequencies correspond to electron beams propagating through the solar corona before they reach interplanetary space.

The focus of this review is to cover the advances in type III theory that have arisen due to new high resolution imaging spectroscopy which became available in the last decade. Type III observations in the past were either analyzed spectroscopically or through imaging only at a few discrete frequencies. Now orders of magnitude better spatial, spectral and temporal resolution is allowing the physics of the radio Sun to be examined like never before. The main telescopes that have been facilitating new type III observations of the Sun are (in descending frequency) the upgraded Karl G. Jansky Very Large Array (VLA, Perley et al., 2011), the Mingantu Ultrawide Spectral Radiograph (MUSER, Yan et al., 2009), the Murchison Widefield Array (MWA, Lonsdale et al., 2009), the Low Frequency Array (LOFAR, van Haarlem et al., 2013) the Long Wavelength Array (Ellingson et al., 2009). Additionally, imaging at discrete frequencies has been provided by the Nançay Radiograph (NRH, Kerdraon and Delouis, 1997) and the Giant Metrewave Radio Telescope (GMRT, Swarup et al., 1991).

This review is not intended to be a historical overview on type III bursts, nor a review of all type III properties. In science we are all “perched on the shoulders of giants” and so readers are encouraged to get a more complete understanding of the field by reading the introductions that are contained within the cited works. There are also many other reviews specifically on type III bursts (Suzuki and Dulk, 1985; Reid and Ratcliffe, 2014) and more generally on solar radio emission (e.g., Dulk, 1985; McLean and Labrum, 1985; Bastian, 1990; Pick and Vilmer, 2008; Gary et al., 2018).

Over the last decade, snapshot synthesis imaging techniques have substantially improved for generating solar radio images. A significant upgrade was made the VLA, described in Perley et al. (2011), where state-of-art receivers and electronics were added, greatly increasing capabilities. There are now a larger number of spectral channels, a larger instantaneous bandwidth for imaging and a faster sampling times, enabling new solar radio observations first documented by Chen et al. (2013). Additionally new radio telescopes like LOFAR, MUSER, and the MWA have been built with large numbers of antenna distributed across large spatial scales. These new telescopes have drastically improved the UV coverage available for making solar imaging spectroscopy, leading to temporal resolution for imaging of 100 ms or better, and for spectroscopy it can go down to microsecond resolution. The increased number of long distance baselines provides orders of magnitude better spatial resolution although radio transport effects limit the use of such high resolution for solar science at MHz frequencies. New and improved telescopes have enhanced spectral resolutions, with low frequencies especially going down to 100s kHz resolution. The latter is particularly significant as previous low frequency imaging spectroscopy has been carried out with spectral resolution of 40 MHz till the 1980s, preventing past imaging spectroscopic analysis of type III fine structure. An example of new imaging techniques using the MWA is given by Mohan and Oberoi (2017).

As well as traditional interferometric techniques, new radio interferometers are able to operate in a coherent tied-array mode that involves combining the collecting area into array beams, or a coherent sum of multiple station beams (see e.g., Stappers

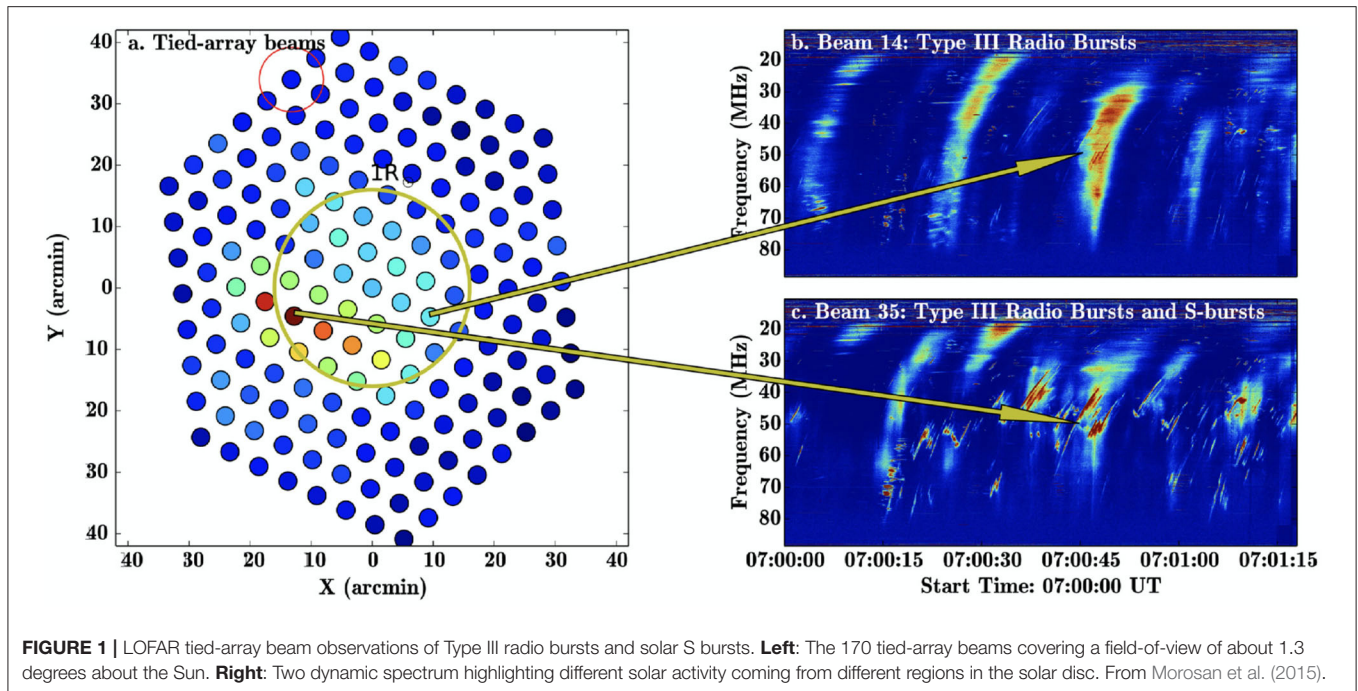
et al., 2011, for a description using LOFAR). Hundreds of tied-array beams are pointed at the Sun in a honeycomb pattern that mosaics the solar radio intensity. The advantage of this method of imaging is enhanced spectral resolution of 10s kHz and temporal resolutions of ms, which are particularly important for imaging type III bursts that are short-lived and change significantly with frequency. The disadvantage is a reduced spatial resolution. An early example of tied-array imaging performed by LOFAR is given in **Figure 1**. This example highlights the power of imaging spectroscopy as each pixel has an associated dynamic spectrum. One is able to disentangle each burst from the other via their spatial information which would not have been possible from full-disc integrated dynamic spectra.

With the successful launch of Parker Solar Probe (PSP, Fox et al., 2016) and Solar Orbiter (SolO, Müller et al., 2013) traveling close to the Sun, analysis of coronal magnetic connectivity is hugely important. In particular with PSP, analysis of *in situ* data close to the Sun is dramatically improved once we know where on the solar disc the plasma originated from. Type III imaging spectroscopy from Earth plays a crucial role here as radio bursts can isolate where high energy particles were accelerated and what trajectory they took when escaping the Sun. Despite energetic protons not producing radio emission, they are likely to follow the same magnetic connectivity as the electrons. Similarly, type III bursts can show the trajectory of heated plasma jets, typically observed in UV or X-rays, which can subsequently be observed *in situ*. Type III bursts are also able to ascertain coronal plasma parameters in high regions of the solar corona (around 1 solar radius and above), where UV and X-ray diagnostics are not effective due to the tenuous plasma not emitting enough photons at these wavelengths. Coronal parameters deduced from type III imaging spectroscopy can then be compared with solar wind parameters detected *in situ* to help understand how the solar corona transitions into the solar wind.

This review begins by discussing high frequency radio bursts and the constraints they make for particle acceleration. Recently observed properties of low-frequency bursts are then discussed in the frame of particle propagation through the corona, along with new type III fine structure observations. The type III contribution toward coronal density models is then featured, along with the difficulties that result from radio wave propagation effects. New insights about electron beams, Langmuir waves and radio waves from recent theoretical models are then presented. The review concludes with a summary of some future observatories and scientific questions that type III imaging spectroscopy can help answer.

## 2. HIGH FREQUENCY BURSTS

Type III bursts observed at high frequencies are signatures of electron transport in the low corona. The term “high frequency” is subjective, and in this context we consider the frequency range of 2–0.2 GHz, with imaging spectroscopy available from the VLA, the NRH and the GMRT. This relates to altitudes lower than roughly 0.5 solar radii from the solar surface (e.g., Newkirk, 1961; Saito et al., 1977) although care must be taken



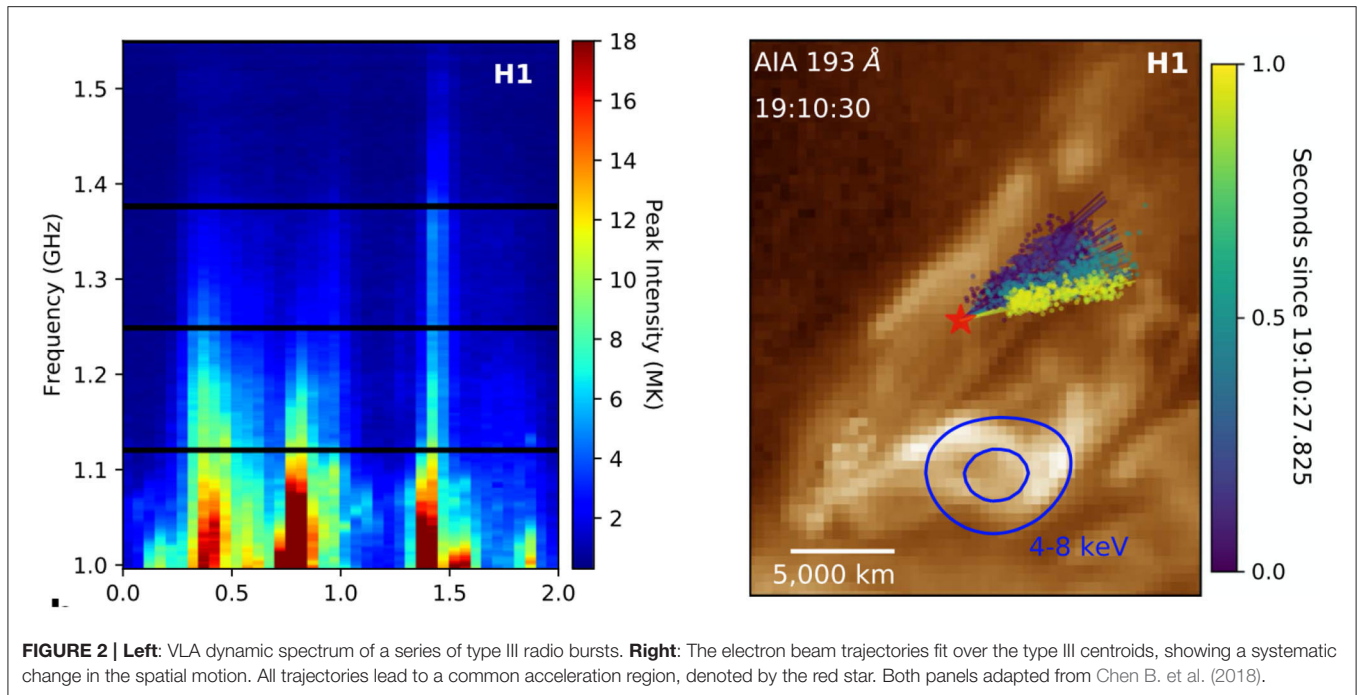
when assuming heights from density models. For example, type III bursts can be observed in the GHz frequencies which requires either active Sun coronal density models or some multiplicative of quiet Sun models.

The importance of analyzing type III bursts at high frequencies is that electron beams which produce the emission have not traveled far from their acceleration region. The electron beams have not undergone significant transport effects and so their kinetic profile as deduced from the type III emission is closer to the acceleration region characteristics that generated them. Solar particle acceleration region characteristics are ill-quantified, and a subject of intense study, because the energized particles propagate away before generating significant electromagnetic emission (see e.g., Zharkova et al., 2011, as a review). This makes high frequency type III burst imaging spectroscopy attractive for diagnosing the spatial, energetic and temporal profile of electron acceleration in the corona.

High resolution type III imaging spectroscopy in GHz frequencies have been carried out using observations from the VLA. Type III bursts were imaged in the low corona, in association with coronal jets (Chen et al., 2013; Chen B. et al., 2018). The evolution of type III source location with frequency was used to estimate the background density profile, assuming second harmonic emission due to low polarization degree. Best-fit density scale heights were derived to be 40 Mm (Chen et al., 2013) and 3–17 Mm (Chen B. et al., 2018), or 5–29 Mm taking into account a 60 degree inclination angle. These are very steep density profiles when one considers that the scale height for a 2 MK plasma is 94 Mm, and likely highlight that the flux tubes are far from their hydrostatic state or highly dynamic in nature. Assuming a density model, the electron beam acceleration site was estimated to be 15 Mm below the 2 GHz

type III emission detected in Chen et al. (2013). The acceleration site was estimated even closer (1 Mm at closest approach) in Chen B. et al. (2018) using the conjunction of varying straight line trajectory fits through the type III centroids at different frequencies (see Figure 2). The different trajectories varied systematically over each 50 ms timestep of the VLA observations and diverged from a compact ( $<600 \text{ km}^2$ ) region. The authors suggest that the very short acceleration timescales strongly favor a reconnection-driven particle acceleration mechanism (e.g., Drake et al., 2006) and estimate a lower limit of  $E > 0.1 \text{ V m}^{-1}$  if a macroscopic DC electric field is responsible. Moreover, by extrapolating their density models back into the acceleration region, a high level ( $\Delta n/n > 100\%$ ) of density inhomogeneity is inferred.

Other high frequency type III imaging observations have been recently analyzed using the GMRT and the NRH. An example using the GMRT found type III emission observed at 610 MHz during a GOES C-class flare (Bisoi et al., 2018). Whilst radio emission was imaged close to the flaring site, a remote source 500 arcsecs away also glowed brightly. The authors confirmed the source was generated by plasma emission and explained the remote source through wave ducting. They also highlighted that a clearer picture could be found if high spectral resolution imaging spectroscopy had been available. An example using the NRH analyzed type III emission before a large coronal mass ejection (Carley et al., 2016). By combining the NRH imaging spectroscopy with radio spectroscopy at higher frequencies, Carley et al. (2016) identified where and when electron acceleration to  $>75 \text{ keV}$  took place, deducing either tether-cutting or flux-cancellation type reconnection at the flux rope center. As the flux rope erupted, it caused reconnection to take place in a fan-spine null point above the rope, producing

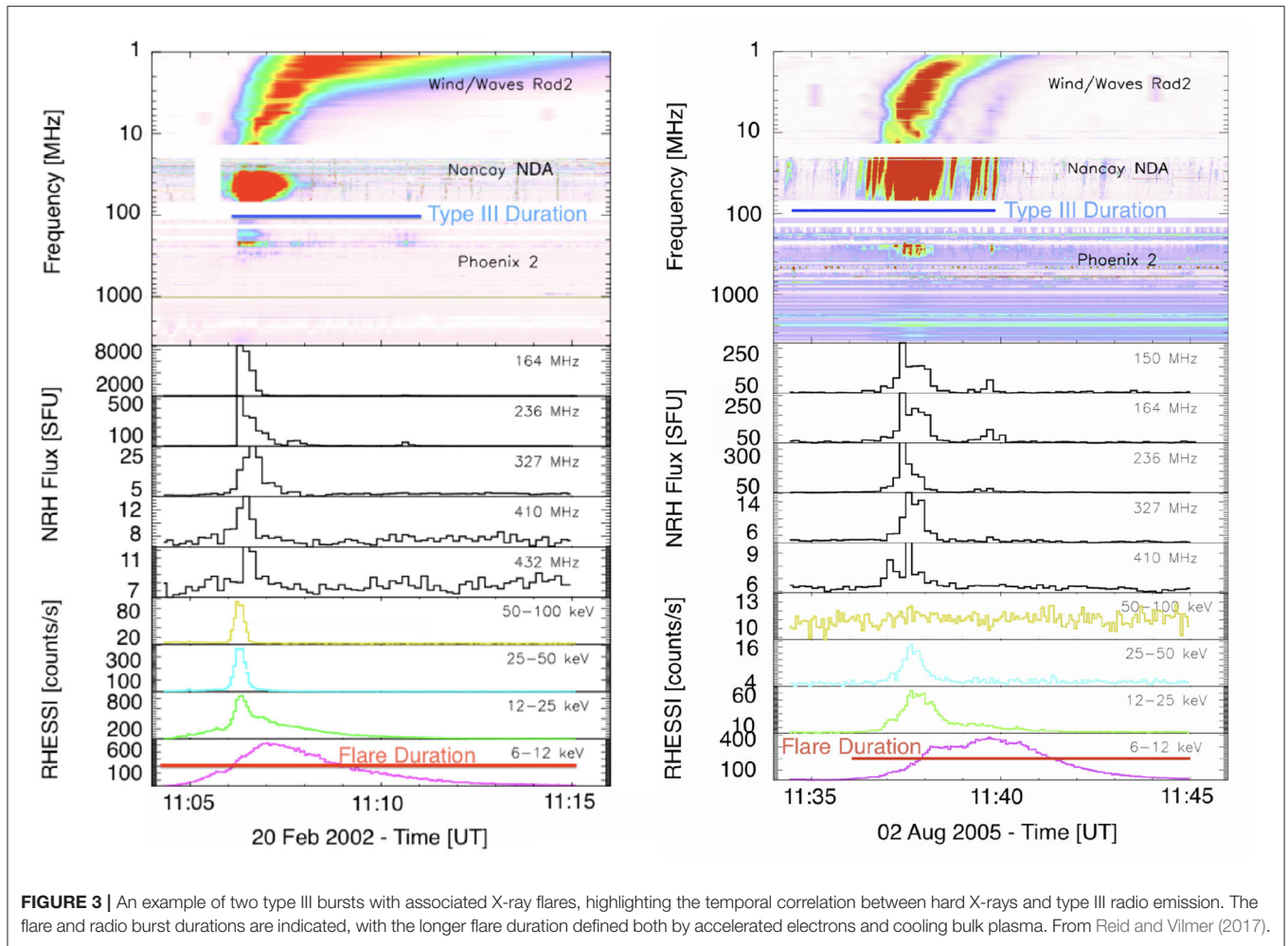


many electron beams around 5 keV for a period of 5 min which caused lower-frequency type III bursts.

All the type III studies above have simultaneous X-ray sources, indicating bi-directional electron beam acceleration. When co-temporal images were available, they provided an impression of the locality of the flare acceleration region and a sense of scale, particularly in Chen B. et al. (2018). Simultaneous study of type III radio and X-rays (see e.g., Pick and Vilmer, 2008, as a review) is attractive because electron beam characteristics can be obtained from the X-ray emission (Holman et al., 2011) and applied to the type III producing electron beams by assuming a common acceleration region. As an example, the distance an electron beam must travel before a “bump-on-tail” distribution forms and it becomes unstable to the production of Langmuir waves has been postulated to be  $\Delta r \approx d\alpha$ , where  $d$  is the longitudinal extent of the acceleration region and  $\alpha$  is the electron velocity spectral index (Reid et al., 2011). This was shown through a correlation between X-ray spectral index with the type III starting frequency (Reid et al., 2014) such that the “soft-hard-soft” pattern of X-ray spectral index was mirrored by a “low-high-low” pattern in the type III starting frequency. The compact acceleration region of  $< 600 \text{ km}^2$  estimated from Chen B. et al. (2018) fits this picture if the instability distance is on the scale of megameters. Additionally, the same physical arguments infer that the electron beam instability distance is also connected to the temporal evolution of the flare acceleration, so as to also be dependent upon  $\Delta r \approx \nu\tau\alpha$  for a characteristic beam velocity  $\nu$ , where  $\tau$  is the characteristic temporal injection time (Reid and Kontar, 2013). The fast type III time profiles on the order of 50 ms shown by Chen B. et al. (2018) infer similar acceleration timescales, which are consistent with the small instability distances of megameters

assuming beam velocities around 0.3c. The combined type III and X-ray flare study by Reid et al. (2014) was also able to estimate acceleration region spatial characteristics, with altitudes ranging from 25 to 200 Mm and longitudinal extents ranging from 2 to 13 Mm.

The temporal correlation between hard X-ray (HXR) bursts and type III radio emission is well-established, being shown in many single-event studies and backed up by statistical studies (Kane, 1972; Kane et al., 1982; Hamilton et al., 1990; Aschwanden et al., 1995; Arzner and Benz, 2005; Reid et al., 2014; Reid and Vilmer, 2017). **Figure 3** shows two examples of flares with temporally correlated radio and X-ray emission. Nevertheless, such a correlation is not present in all flares, presumably relating to different magnetic connectivity preventing electron beams to simultaneously stream down into the chromosphere and up into the higher corona. A statistical correlation over 10 years of type III events with co-temporal X-ray flares has been found between the peak type III flux and the peak X-ray count rate using imaging spectroscopy from the NRH to obtain the type III flux profile (Reid and Vilmer, 2017). Whilst a large amount of non-thermal X-ray counts were accompanied by high flux type IIIs, a low amount of non-thermal X-ray counts was accompanied by both high and low flux type IIIs. This result is explained by low density electron beams being able to produce detectable type III bursts via the amplification of coherent waves. Conversely, a high number of hard X-rays counts is dependent upon high beam densities due to the incoherent nature of Bremsstrahlung (Holman et al., 2011; Kontar et al., 2011). The dependency of hard X-rays on the number of high energy electrons naturally explains the notable absence of events with high X-ray intensity and low type III radio flux. This is another reason that co-temporal type III bursts and HXRs are not observed during all flares.



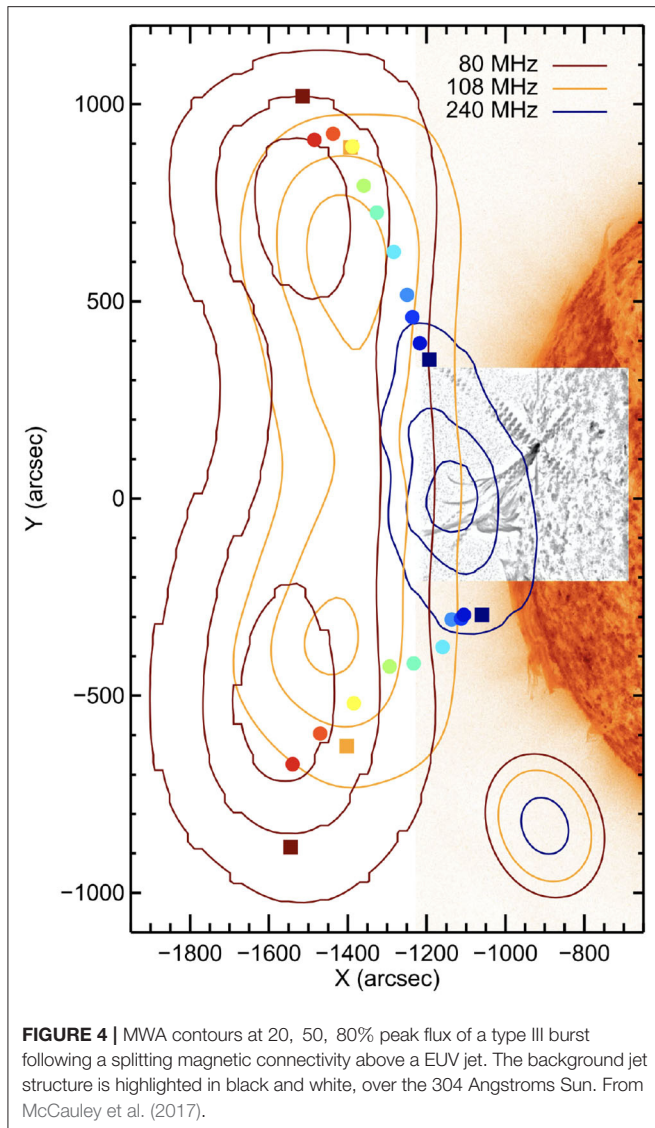
Electron beams that propagate down through the dense corona can also produce reverse type III bursts, which have corresponding positive frequency drift rates and typically start at frequencies  $>500$  MHz (Islaker and Benz, 1994; Aschwanden and Benz, 1997). Simultaneous type III and reverse type III events are of particular interest for new-age imaging spectroscopy studies at higher frequencies because the radio positions localize the acceleration region which must be situated between the standard and reverse type IIIs. These bi-directional type III events are a key motivation for simultaneous imaging spectroscopy between 1 GHz and 100 MHz with high frequency resolutions. Currently, it is typical that only one side (normal or reverse) of the bi-directional burst is imaged (e.g., Feng et al., 2016). A wide range of bi-directional type III properties were reported by Tan et al. (2016) using radio spectroscopic observations. Using the full MHD equations and an assumption of a barometric atmosphere, Tan et al. (2016b) devised a model where the electron beam velocity can be estimated using the plasma beta and the type III drift rates. By estimating the plasma temperature (e.g., using soft X-ray line ratios), the upper and lower estimates of electron beam velocity can be used to obtain estimates of the magnetic field at densities

corresponding to the start frequencies of the bi-directional type III bursts. The magnetic field of the acceleration region is then simply assumed to be an average of these two values, with estimates found between 50–90 G and 4–18 G for two events (Tan et al., 2016a).

### 3. LOW FREQUENCY BURSTS

Type III bursts at the low frequencies are signatures of electron beams traveling through the high corona before they reach the solar wind. In this section we define “low frequency” from around 200 MHz down to 10 MHz, the frequency at which Earth’s ionosphere becomes opaque to solar radio emission, with imaging spectroscopy results mainly from LOFAR and the MWA.

Low frequency type III radio emission provides diagnostics of electron beams that have propagated into the upper solar corona. The electron beams have undergone more propagation effects than when they produce the high frequency type III components, and so low frequency type IIIs are a key source of electron transport diagnostics. Electron beams that produce low frequency type IIIs are likely to propagate out of the



solar atmosphere and therefore their presence indicates coronal magnetic field lines open to the solar wind. As such, low frequency type IIIs provide an important diagnostic of magnetic field connectivity for solar wind and space weather studies, provided they are corrected for radio propagation effects. The higher the flux of low-frequency type III emission, as found from NRH imaging spectroscopy at 150 MHz, the more likely that an interplanetary type III burst is observed (Reid and Vilmer, 2017), with almost all sampled type III events with flux greater than 1000 SFU generating interplanetary bursts.

Type IIIs are commonly associated with jets in extreme ultraviolet (EUV) and X-rays (e.g., Bain and Fletcher, 2009; Klassen et al., 2011; Krucker et al., 2011), with electron beams typically following the same path as the jet. A number of studies have analyzed type IIIs using high resolution MWA imaging spectroscopy that occurred co-temporal and co-spatially with jets observed in UV (McCauley et al., 2017; Cairns et al., 2018;

Mulay et al., 2019). In all three events the type III emission showed resolved fine temporal structure, consistent with several distinct EUV jet episodes and caused by multiple electron beam injections, explained via energization within magnetic reconnection regions by Cairns et al. (2018). A splitting of the magnetic connectivity was highlighted by McCauley et al. (2017) using MWA imaging spectroscopy of a succession of type III radio bursts. The radio bursts started from a common source around 200 MHz and split into two separate sources, following different magnetic flux tubes. The UV jet traces out a region where the magnetic field connectivity diverges, which appears to facilitate the splitting of the type III into two separate sources, indicated in **Figure 4**. For this event, type III imaging spectroscopy was used to ascertain typical electron beam speeds around 0.2c. Comparing with magnetic field extrapolations, Mulay et al. (2019) found type III radio sources at the flaring site which did not appear at the expected points along magnetic field lines. There was a distinct absence of type III frequency evolution along the field that would be consistent with electron beam propagation. Mulay et al. (2019) concluded this was possibly due to radio wave scattering or the magnetic field extrapolation not including local small scale variations.

Not all electron beams that generate type III bursts are able to escape into the solar wind. Some electron beams travel along loops that are confined to the corona, producing radio emission that forms a J- or U-shape in the dynamic spectrum, known as J/U-bursts (Maxwell and Swarup, 1958). J-bursts can also occur at the same time as coronal jets, with one imaged using LOFAR by Morosan et al. (2017) where the accelerated electron beam traveled along a large magnetic coronal loop. The electron beam can also mirror at the footpoint of magnetic loops forming what is known as an N-burst, with Kong et al. (2016) reporting a well-observed N-burst using the NRH. The bulk of magnetic flux is closed in the corona and so we might expect U-bursts and J-bursts to be observed more often than type III bursts when in fact the converse is true. Using the derived magnetic loop and electron beam parameters from LOFAR imaging spectroscopy, Reid and Kontar (2017a) analyzed the electron beam instability criteria, shown in **Figure 5**. For radio emission to be generated on closed magnetic fields, the loop needs to be long enough for a power-law accelerated electron beam to become Langmuir-wave unstable through time-of-flight. Additionally the beam needs to be dense enough for the timescale of Langmuir wave growth and their successive conversion to radio waves to be shorter than the electron propagation timescale. These conditions result in a stricter set of requirements for electron beams and background loop plasma parameters to produce U/J-burst radio emission over type III radio emission.

One quintessential property of type III radio bursts is the frequency drift rate, typically attributed to the bulk speed of the electron beam traveling through the solar plasma. The enhanced spectral resolution from LOFAR and the MWA allows drift rates to be more accurately measured and has been statistically sampled recently by a number of radio spectroscopic studies by Morosan and Gallagher (2017) and Reid and Kontar (2018a) that used LOFAR, by Zhang et al. (2018) that used the Nançay Decametre Array (NDA, Lecacheux, 2000), and by Stanislavsky

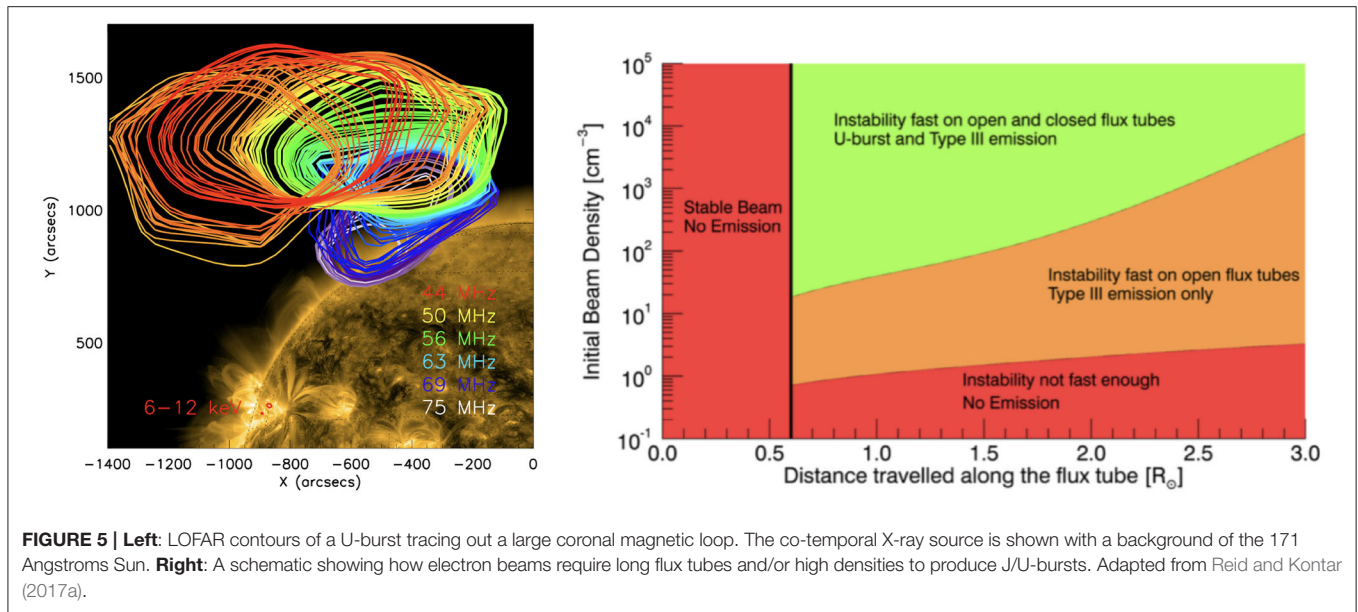


**FIGURE 5 | Left:** LOFAR contours of a U-burst tracing out a large coronal magnetic loop. The co-temporal X-ray source is shown with a background of the 171 Angstroms Sun. **Right:** A schematic showing how electron beams require long flux tubes and/or high densities to produce J/U-bursts. Adapted from Reid and Kontar (2017a).

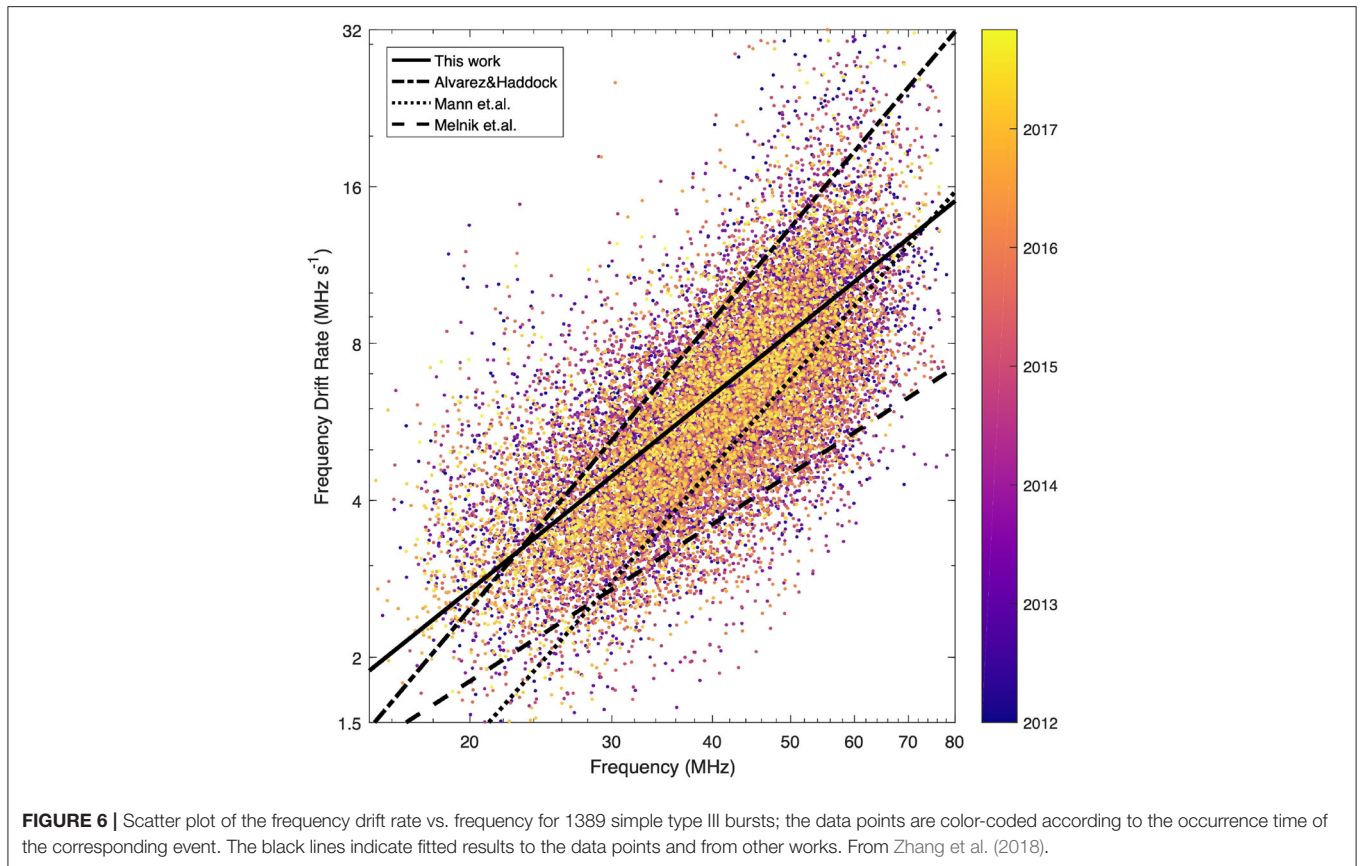
et al. (2018) that used the Ukrainian T-shaped Radio telescope (UTR-2, Konovalenko et al., 2016). Similar to Alvarez and Haddock (1973) who compared type III drift rate from 550 MHz to 50 kHz from many studies, the drift rate has been approximated by a power law of the form  $\frac{\partial f}{\partial t} = -Af^\alpha$ . Findings for  $\alpha$  were  $-1.82 \pm 0.11$ ,  $-1.63 \pm 0.11$ ,  $-1.23$ ,  $-2.11 \pm 0.66$ , respectively for the four studies, compared to the value of  $\alpha = -1.84$  found by Alvarez and Haddock (1973). It is unsurprising that the power law spectral indices vary because the type III drift rate depends primarily upon the speed of the electron beam exciter (e.g., demonstrated numerically by Reid and Kontar, 2018b), the density gradient of the background plasma, and whether the radio burst was generated via fundamental or second harmonic emission. For fundamental emission, the electron beam travels smaller distances over the same frequency range. Moreover, the fundamental emission is more susceptible to radio wave propagation effects (see section 3.3).

It is noteworthy that Zhang et al. (2018) found such a low spectral index as they sampled nearly 1400 type III bursts over half a solar cycle via an automatic analysis system using a Hough transform. **Figure 6** shows a scatter plot of the frequency drift rates, highlighting the huge spread in values between different radio bursts. If we assume that the background electron density was similar for all studies, as was the proportion of fundamental to harmonic emission then Zhang et al. (2018) observed more electron beams with lower bulk velocities than the other studies. Lower velocity beams take longer to travel from one frequency to another and hence the frequency drift rate is smaller in magnitude. The large number of type IIIs detected by the automated method might have analyzed a greater number of type IIIs with low signal-to-noise ratio, produced by slow, weak beams, which may account for the lower magnitude drift rates observed. A similar study would be beneficial using new type III imaging spectroscopy from telescopes with larger

collecting areas to detect very faint type III bursts and make a drift rate comparison between them and the type III bursts with higher fluxes.

The time profile of type III bursts is another property that has undergone recent analysis. At a single frequency, the time profile is influenced by a convolution of processes based upon the plasma emission mechanism including; beam acceleration characteristics, beam velocity dispersion, the radio emission process, radio propagation, and density variation in the solar corona. Characterizing when certain processes are dominant is essential for extracting diagnostic information about the electron beam. The high flux sensitivity and time resolution of new type III imaging spectroscopy makes it ideally suited for analyzing the rise and decay of type III emission at a single frequency. At frequencies between 30-70 MHz, Reid and Kontar (2018a) used LOFAR to analyzed 31 radio bursts, coming to the conclusion that their half-width half-maximum (HWHM) rise and decay was best fit by a Gaussian rise plus a Gaussian decay. This was the first study to analyse the type III HWHM rise time, finding  $t_{\text{rise}} \propto f^{-0.77 \pm 0.14}$ . The Gaussian decay was in contrast to the exponential decay used in previous works (e.g., Aubier and Boischoit, 1972; Barrow and Achong, 1975; Mel'Nik et al., 2011) although similar HWHM decay times were found. The decay time  $t_{\text{decay}} \propto f^{0.89 \pm 0.15}$  compares very well with comparisons of decay times all the way down to kHz frequencies, shown by Kontar et al. (2019), that could be fit with a power-law that had a spectral index close to 1. The rise and decay times also showed a very strong correlation, indicating that one process dominates both time scales at LOFAR frequencies.

The explanation put forward by Reid and Kontar (2018a) is that the rise and decay times are primarily caused by the front and back of the electron beam, respectively, separated through velocity dispersion. The front of the electron beam consists of faster particles and so consequently they arrive at a



certain background plasma frequency first. Similarly the back of the electron beam is made up of slower particles and so arrives last. This theory was consistent with the larger and smaller magnitudes of drift rates found using the rise and decay time, respectively (Reid and Kontar, 2018a) and with quasilinear simulations (see section 4). Assuming a coronal density model gave average front and back velocities of  $0.2 \pm 0.06c$  and  $0.15 \pm 0.04c$ . The same conclusion was obtained by Zhang et al. (2019) who used LOFAR imaging spectroscopy to analyse one radio burst. They found the source locations from the rise, peak and decay times were displaced with respect to one another, and followed different paths in the solar atmosphere. Derived velocities from centroid locations were different, with the velocities relating to the front edge, peak and back edge of a type III burst were  $0.42c$ ,  $0.25c$ , and  $0.16c$ , respectively. The centroids of the front edge were farther away from the solar disc meaning that the front of the electron beam was propagating along a magnetic flux tube with higher coronal density whilst the back of the beam was propagating along a flux tube with lower coronal density. It seems that whilst the rate of velocity dispersion is governed by the electron beam acceleration characteristics like energy spectral index, the magnetic flux tubes that guide electron beams also influence the type III durations.

Velocity dispersion is not the only effect that contributed to type III durations, and Zhang et al. (2019) estimated the contribution of density turbulence and wave propagation effects.

Density variation causes different regions in the solar atmosphere to have the same plasma frequency, and hence contribute to the time profile at any given frequency (Roelof and Pick, 1989). By analyzing the wave frequency distribution of sources observed at the same distance from the solar disc, Zhang et al. (2019) estimated the effect of density variation, finding that it caused an observed duration about 2.2–5.7 times the duration caused by density variations (a lower effect than, Roelof and Pick, 1989). Wave propagation effects were also analyzed using shorter duration type III bursts occurring before the main type III burst. These provided an upper limit on the effect of wave propagation effects of less than half of the observed duration. Whilst the growth rates of radio waves from Langmuir waves are fast, more theoretical study should be carried out to fully explore the effect of the radio emission mechanism on the type III drift rates.

Type III polarization measurements are a strong diagnostic potential for discerning between fundamental and harmonic emission. There has not been much recent works using polarization information in imaging spectroscopy as calibration issues complicate matters. A recent work (Rahman et al., 2020) looked at the polarization of type IIIs using the MWA. They found the degree of circular polarization increased as a function of frequency and was higher at the start of the radio bursts, consistent with previous models that fundamental emission is generated first. The polarization fraction decreased with time, consistent with scattering effects depolarizing the radio emission.

### 3.1. Fine Structure

One of the most powerful applications of high resolution imaging spectroscopy lies in the analysis of fine structure. For type III bursts this typically takes the form of striae bursts, or type IIIb bursts (de La Noe and Boisshot, 1972), fine structure exhibited along a backbone of fundamental emission. The general consensus about the driver is density turbulence in the background plasma (e.g., Takakura and Yousef, 1975) although a formal theoretical treatment of the entire process is yet to be formulated. With previous imaging, the spectral resolution was too sporadic to have multiple images of one stria. A number of studies using LOFAR imaging spectroscopy (Kontar et al., 2017; Chen X. et al., 2018; Kolotkov et al., 2018; Sharykin et al., 2018) have analyzed striae bursts, concentrating on one specific event on the 16 April 2015.

The LOFAR dynamic spectrum and corresponding image is shown in **Figure 7**. Kontar et al. (2017) concentrated on analyzing the spatial information of individual striae. They found that individual striae increased in size at a single frequency, and this rate was different between the fundamental and harmonic emission. They reasoned that the intrinsic source size (the actual size of the source in the corona) is much smaller than the apparent source size (source size derived from radio waves at Earth) and hence the brightness temperature of the sources is orders of magnitude larger than what is estimated using observed source size. The power spectral density of the same type IIIb burst was analyzed by Chen X. et al. (2018). They found that the fluctuations had an almost 5/3 spectral index in wavenumber space, similar to what is normally observed for solar wind density turbulence at 1 AU (Chen, 2016). Interestingly the same spectral index was found for the harmonic emission, possible to obtain due to the sensitivity and the spectral resolution of LOFAR. A characteristic spatial scale of striae was estimated around 700 km, using the Newkirk density model (Newkirk, 1961) rather than spatial positions because the source was located over the solar disc. Sharykin et al. (2018) extended this study to analyse the spatial motion of the individual striae. These structures have an instantaneous bandwidth around 20–100 kHz that increases with increasing central frequency. By fitting each striae with a elliptical Gaussian, they found the striae drift rate around 0–0.3 MHz s<sup>-1</sup>, increasing with increasing central frequency. The mean striae speed from the drift rate was around 600 km s<sup>-1</sup>, larger than the typical sound speed of 200 km s<sup>-1</sup> and smaller than the type III burst speed of 0.2c. Kolotkov et al. (2018) analyzed the same type III event, finding quasi-periodicity in the signal. The authors explained the periodicity by a propagating fast wave train that modulated the radio emission produced by the electron beam.

Spectroscopic observations of type IIIb bursts have been carried out by Tun Beltran et al. (2015) using the LWA. Analyzing a type III storm that displayed both type IIIs and type IIIbs, they concluded that electron beams must travel along magnetic structures with density inhomogeneities present. Moreover, the sudden onset of type IIIb storms from a normal type III storm must be explainable, which could be caused by different electrons propagating along different magnetic field lines with an increased level of density turbulence. Mugundhan et al. (2017) also spectroscopically analyzed a number of type IIIb

bursts using the Guribidanur Low Frequency Solar Spectrograph (GLOSS, Kishore et al., 2014). By analyzing numerous striae, they approximated  $\Delta n/n$  using the observed value of  $\Delta f/f$ , finding ranges of  $0.006 \pm 0.002$ . Sharykin et al. (2018) made the same assumption and found similar amplitudes of  $10^{-3}$ .

### 3.2. Coronal Density Models

The advent of high resolution imaging spectroscopy has brought increased interest in using type III bursts to diagnose the density structure of the solar corona. Type III frequencies are associated with a background electron density assuming either fundamental or second harmonic emission. The change in centroid position of the type III sources as a function of frequency thus provides information about how the background coronal density changes with altitude,  $n_e(r)$ . Altitudes inferred from type IIIs are typically larger than altitudes predicted by standard coronal density models. Previous investigations using spectra and images at a few frequencies explained the enhanced altitudes through type IIIs being generated in over-dense structures (e.g., Wild et al., 1959; Trotter et al., 1982; Kundu et al., 1983) as there were spatially correlated streamers imaged in white light. An alternative explanation is that the enhanced altitudes are not real. Radio source centroids are shifted by scattering of radio waves off density inhomogeneities, which causes their apparent position to be farther away from the Sun (e.g., Riddle, 1974). This theory is currently preferred as many type III bursts are not necessarily observed over dense streamers (e.g., Leblanc and de La Noe, 1977). The reality is likely that both scenarios are possible, with some proportion of type III events occurring on over-dense flux tubes. A nice historical overview on some issues arising from coronal density models derived from type IIIs is given in McCauley et al. (2018).

The initial results from LOFAR imaging spectroscopy were consistent with previous findings that type III sources corresponded to altitudes much higher than standard coronal density models would infer (Morosan et al., 2014), with altitudes extending out to 3 solar radii around 30 MHz. This was significantly farther out than predicted by a density model using white-light data from the same day (Zucca et al., 2014). Further observational studies using the MWA and LOFAR found altitudes deduced from type III observations to be much higher than standard coronal density models predicted (Reid, 2016; Mann et al., 2018; McCauley et al., 2018; Gordovskyy et al., 2019). **Figure 8** shows an example of such a density model being found from type III centroid locations. Whilst it might be possible that type IIIs preferentially travel along over-dense flux tubes, the electron beam velocities that can be deduced from type III bursts must also be consistent with theory. Some deduced velocities from type III bursts observed by LOFAR were found to be superluminal (Reid, 2016; Mann et al., 2018). Such velocity estimates are likely influenced by the spatial and temporal modifications due to radio wave propagation effects (see section 3.3) but other effects may also play a role such as different regions of the electron beam emitting radio waves at different times, creating an apparent speed faster than the beam speed (Reid and Kontar, 2018b). Other deduced velocities by LOFAR and the MWA using imaging spectroscopy have been

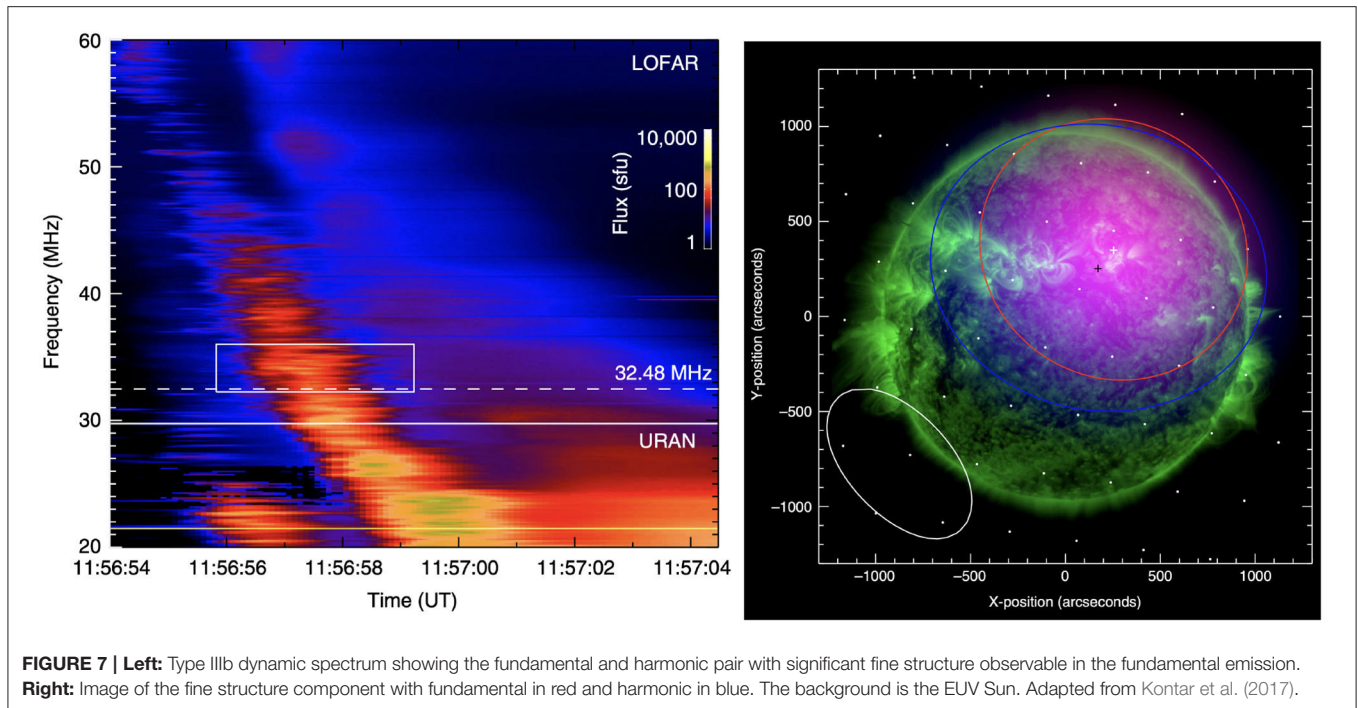


**FIGURE 7 | Left:** Type IIIb dynamic spectrum showing the fundamental and harmonic pair with significant fine structure observable in the fundamental emission. **Right:** Image of the fine structure component with fundamental in red and harmonic in blue. The background is the EUV Sun. Adapted from Kontar et al. (2017).

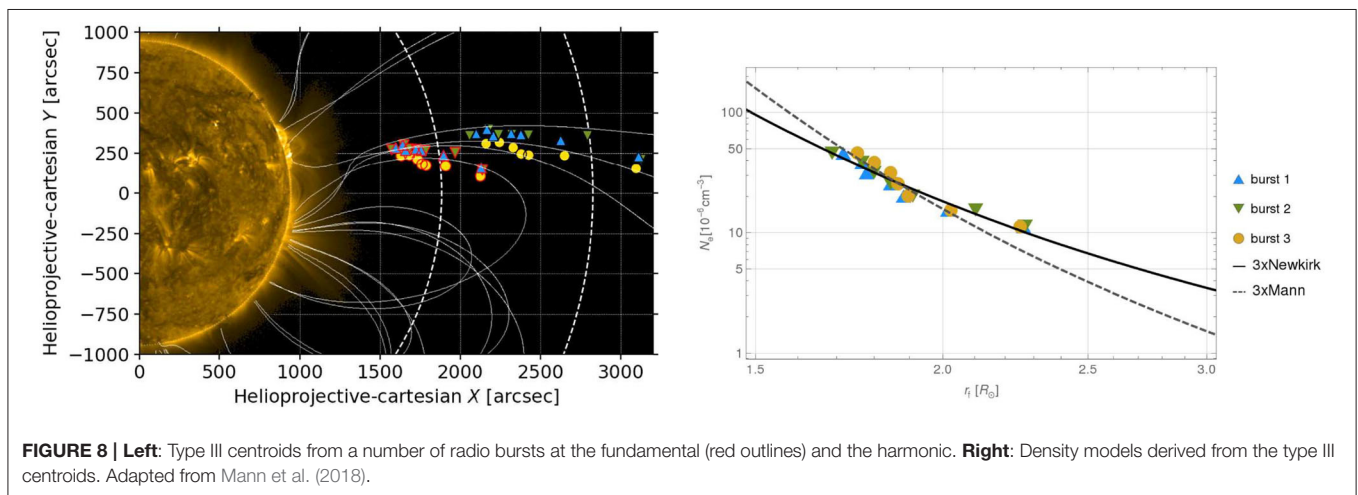


**FIGURE 8 | Left:** Type III centroids from a number of radio bursts at the fundamental (red outlines) and the harmonic. **Right:** Density models derived from the type III centroids. Adapted from Mann et al. (2018).

higher than the standard 0.1-0.3c velocities typically observed (e.g., Morosan and Gallagher, 2017; McCauley et al., 2018).

Type U and J bursts allow diagnosis of coronal densities within magnetic flux tubes confined to the corona. Using LOFAR, Reid and Kontar (2017a) found the coronal density profile from two J-bursts and one U-burst that occurred in quick succession. Estimating second harmonic emission, the density profile roughly fit enhanced standard density profiles, the  $3.0\times$  Baumbach-Allen Model (Allen, 1947),  $3.5\times$  Sittler model (Sittler and Guhathakurta, 1999) and  $4.5\times$  Saito Model (Saito et al., 1977) density model. However, the lowest frequencies around 40 MHz at the loop apex did not fit any density models as the magnitude of the density gradient became much less at these frequencies. Only by taking into account this change in density

gradient obtained through the imaging spectroscopy were realistic burst exciter speeds around 0.2c able to be estimated.

Radio observations taken only from the Earth suffer from projection effects; our limitation of imaging on a 2-dimensional plane without any spatial information on the line-of-sight dimension. Projection effects can only amplify the larger derived electron density altitudes from type III bursts, getting larger the more the electron beam is propagating toward/away from the Earth. The uncertainty is amplified for electron beam source regions that are close to the center of the Sun. An example was shown by Gordovskyy et al. (2019) on how projection effects modify derived density models using LOFAR imaging spectroscopy for four different events at electron beam propagation angles of 90, 60, and 30 degrees from the Sun-Earth

line. Most of the sources were off-disc and so 30 degrees gave widely inaccurate frequency vs. distance estimates. Such small projection angles are more likely to occur for on-disc sources close to Sun center. Whilst radio projection effects amplify the larger derived electron density altitudes, the larger the radio projection effect, the smaller the correction for radio wave propagation from source to observer as more of the scattering will occur along the line of sight and so not affect the 2D radio imaging spectroscopy.

### 3.3. Radio Wave Propagation

Understanding the propagation of radio waves through the solar system is paramount if we are to make best use of radio imaging spectroscopy at low frequencies. The displacement of sources by scattering was convincingly shown using LOFAR's high resolution imaging spectroscopy of a type III burst displaying both fundamental and harmonic emission (Kontar et al., 2017). A systematic radial displacement of  $1.8 \text{ arcmin s}^{-1}$  was observed for the fundamental emission. We would expect the fundamental type III emission to be more displaced through scattering off density inhomogeneities because the radio frequency is closer to the local plasma frequency. The radial displacement was found for numerous fundamental emission fine structures (stria) between 32 and 38 MHz. Moreover the areal extent of the fundamental sources increased faster than the harmonic emission at a single frequency, consistent with radio waves scattering off density inhomogeneities. An increase in the area of the burst source was also observed by Mohan et al. (2019) using type III imaging spectroscopy from the MWA. They found a radial expansion around  $43 \text{ Mm s}^{-1}$ , two orders larger than the local Alfvén speed and so rejected the increase in physical area due to magnetic waves. With LOFAR and MWA showing how important radio wave propagation is to the spatial characteristics of fundamental emission, this opens up the ability to test radio wave propagation models (Robinson, 1983; Arzner and Magun, 1999; Thejappa and MacDowall, 2008) and investigate analysis of the turbulent structure of the solar corona. Analyzing the same type III event as Kontar et al. (2017), Sharykin et al. (2018) found that the source size across the line-of-sight exceeds the size along the line-of-sight, implying that radio wave scattering must be anisotropic. Mohan et al. (2019) used the model by Arzner and Magun (1999) on the analyzed type III bursts to estimate a value of  $\Delta n/n = 4 \times 10^{-3}$ .

It is attractive to correct for propagation effects so that type III burst source positions can derive more realistic coronal density models. A method proposed by Chrysaphi et al. (2018) treats radio wave propagation like scattering of a charged particle in plasma. They applied this technique to LOFAR imaging spectroscopy of a type II, showing that split-band emission can arise from the same spatial location. The mean scattering rate depends upon the local intensity of density turbulence and the frequency of radio emission. By integrating over regions where the optical depth is greater than one, a radial correction can be approximated. Chrysaphi et al. (2018) found corrections around  $0.3 \mathcal{R}_{\odot}$  for 40 MHz and  $0.6 \mathcal{R}_{\odot}$  for 32 MHz. The technique was applied to type III emission by Gordovskyy et al. (2019) showing that it can indeed explain larger than

expected heliocentric distances of radio sources. A different correction method was proposed by McCauley et al. (2018) who calculated synthetic radio images using the FORWARD software (Gibson et al., 2016) to find expected Bremsstrahlung and gyroresonance emission from a model atmosphere found using the MAS software (Lionello et al., 2009) to extrapolate coronal magnetic fields and then applying a heating model (Schrijver et al., 2004) to compute density and temperature. The difference between observed type III burst source locations, found using MWA imaging spectroscopy between 80 and 240 MHz, and the synthetic radio images was found to estimate the effect of radio propagation effects. Using three type III radio bursts they found corrections around  $0.3 \mathcal{R}_{\odot}$  for 80 MHz and  $0.1 \mathcal{R}_{\odot}$  for 240 MHz, slightly higher than those predicted by Chrysaphi et al. (2018). Applying the corrections to the estimated coronal density models from type III bursts, McCauley et al. (2018) found a better agreement with typical density models, although two type III bursts had unusually steep density profiles. The third type III burst agreed well with a type III density model predicted by Cairns et al. (2009) from type III burst spectra.

The above methods attempt to approximate the effect of radio wave scattering off density fluctuations but to properly understand this effect, ray-tracing simulations are required. There have been a number of ray-tracing studies in the past that have tracked type III burst propagation (Steinberg et al., 1971; Thejappa and MacDowall, 2008; Krupar et al., 2018) which assumed isotropic scattering by small-scale density fluctuations. Krupar et al. (2018) using the STEREO spacecraft and Krupar et al. (2020) using Parker Solar Probe found that from the arrival time, the exponential decay times observed at low frequencies from spacecraft are able to be explained through the scattering of radio waves by density inhomogeneities. Bian et al. (2019) modeled the scattering process using a Fokker-Planck equation and were able to reproduce the time profile but not the inverse frequency dependence of the decay time, which they concluded was down to the exclusion of a large-scale refractive term. Kontar et al. (2019) recently extended the work of Bian et al. (2019) but treated the scattering in the anisotropic domain, with the dominant effect being perpendicular to the heliospheric radial domain (Kontar et al., 2017). As well as explaining temporal profiles, Kontar et al. (2019) used ray-tracing simulations to explain the increase in source sizes, finding a scattering increase in the FWHM around  $1.1 \mathcal{R}_{\odot}$  at 35 MHz, although this value will depend upon the size of the density fluctuations from event to event. Changing the anisotropy parameter strongly influences source sizes that are off the solar limb and less so at disc center.

## 4. ELECTRON BEAM PROPAGATION

Electron propagation through plasma is the cause of type III radio bursts and there has been an extensive amount of theoretical work on the subject. Electrons have been simulated propagating through the solar coronal plasma and out into the interplanetary medium. Their propagation is not simply ballistic but is modified by the energy exchange with Langmuir waves as the electron beam becomes unstable during transport. The radio

emission is then believed to be mainly produced through wave-wave processes with ion-sound waves to produce fundamental emission, and with almost oppositely directed Langmuir waves for second harmonic emission.

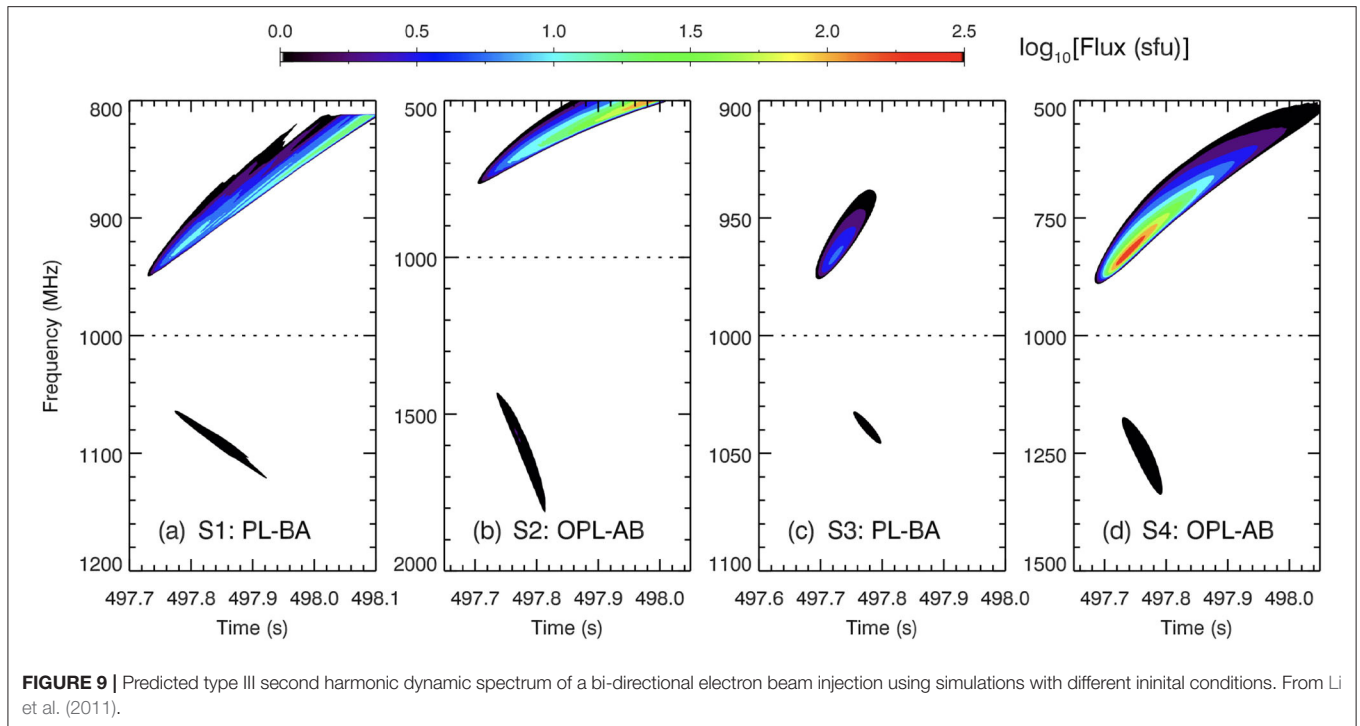
In this section, the recent theoretical progress is discussed that has been undertaken to explain how type III bursts are generated by propagating electron beams. This theoretical understanding is critical for using type III bursts as remote sensors of electron acceleration and propagation through the solar corona and to maximize the research output that we can obtain from Earth-based imaging spectroscopy. It is beyond the scope of this review to cover all simulation works and so, as indicated in section 1, readers are encouraged to look through the introductions contained within cited works to obtain a more historical overview of the subject. In almost all of the work the electron beam acceleration is taken as an initial condition. This is largely due to the complexity and unanswered questions about which mechanism is responsible for electron acceleration in the corona (e.g., Zharkova et al., 2011).

Assuming electron beam acceleration with a power-law energy spectrum, the beam undergoes an initial period of propagation without becoming unstable to Langmuir waves. This “instability distance” is related to the distance required for velocity dispersion to create the bump-in-tail velocity distribution required for Langmuir wave generation. As discussed in section 2, quasilinear simulations (Reid et al., 2011; Reid and Kontar, 2013) showed that the distance is dependent upon the electron beam velocity spectral index, the size of the acceleration site, and the temporal injection profile. The instability distance is the reason that the starting frequency of type III bursts is not observed at the particle acceleration region. Perhaps the most striking observation that shows this are the bi-directional type III bursts where there is a frequency gap, and hence a spatial gap between the forward and reverse type III bursts. The simulations done by Li et al. (2011) show this spatial gap well and highlight the reduced intensity of radio emission generated by electron beams propagating through plasma with a positive density gradient (**Figure 9**). Whilst Li et al. (2011) assumed a 20 MK Gaussian distribution of accelerated electrons, their distribution had a spatial width of 1 Mm which likely influenced the frequency gap between downward and upward propagating electron beams.

Despite electron beams being made up of electrons with a distribution of velocities, type III bursts are typically tracked using one velocity derived by the frequency drift rate. The main theoretical reason behind this pseudo-constant velocity is the beam-plasma structure that is formed by the electron beam wave-particle interactions with Langmuir waves, proposed theoretically (Zheleznyakov and Zaitsev, 1970; Zaitsev et al., 1972; Mel’Nik, 1995) and successfully simulated (Takakura and Shibahashi, 1976; Magelssen and Smith, 1977; Kontar et al., 1998; Mel’Nik et al., 1999). Electrons travel as an ensemble with roughly the mean velocity of all electrons taking part in the energy exchange between waves and particles. Langmuir waves are generated at the front of the beam and re-absorbed at the back of the beam, allowing propagation over long distances of 1 AU, and avoiding a catastrophic beam energy loss postulated by Sturrock (1964).

The initial properties of the accelerated electron beam play a significant role in how the resultant type III burst evolves through the solar corona. Understanding how these properties modify the radio dynamic spectra is key to using type III imaging spectroscopy as a probe of electron beam transport in the solar corona. Assuming that the injected energy spectra is a power-law, the spectral index of this distribution influences which electrons contribute to the beam-plasma structure and therefore how fast the resultant electron beam propagates through space (e.g., Li and Cairns, 2013; Reid and Kontar, 2018b). When simulated, Li and Cairns (2013) found that smaller spectral indices give rise to faster electron beams, cause type III bursts to have higher magnitude drift rates and result in higher peak values of type III burst fundamental emission. However, the electron beam speed is not just governed by the spectral index but by the initial beam density too as both properties govern the energy density contained within the electron beam. It is this energy density that more completely governs which electrons contribute to the beam plasma structure (Reid and Kontar, 2018b). If the energy density is too small at certain electron energies, the Langmuir wave growth rate will not be high enough and these energies will not contribute to the beam-plasma structure that dictates beam speed. As electron beams expand in the solar wind, their energy density decreases and they stop producing radio emission (Reid and Kontar, 2015). Additionally, Reid and Kontar (2018b) showed that the peak brightness temperature of type III fundamental emission is proportional to the energy density contained within the electron beam. This result is significant as, if proven to be true via *in situ* measurements from PSP or SolO, type III bursts can be used to estimate the energy density of beams traveling through the solar corona. Moreover, with electron beam size estimates using type III imaging spectroscopy by taking into account wave propagation effects, the total energy contained within escaping electron beams during solar eruptive events can be estimated.

As discussed from LOFAR observations in section 3, the drift rates at the front of the beam are faster than the drift rates at the back of the beam, relating to faster and slower velocities, respectively (Reid and Kontar, 2018a; Zhang et al., 2019). This dependence was found using numerical simulations by Reid and Kontar (2018b) using the drift rates from synthetic fundamental emission dynamic spectra. The front of the beam was always faster than the back and could travel over twice as fast. The maximum and minimum electron energies in the beam plasma structure were significantly higher at the front than at the back of the beam, and so average velocities greater than  $0.5c$  were possible. This is in stark contrast to the back of the beam, where the minimum energy was dictated by the temperature of the background plasma and so velocities cannot go higher than  $0.5c$ . Simulations from Li and Cairns (2014) showed that higher beam velocities occur when the background plasma is simulated by a kappa distribution as the minimum energy that contributes toward the beam plasma structure is higher. It remains to be proven whether the solar corona can be described by a kappa distribution like the solar wind. The difference between the electron energies at the front and back of the beam dictate how fast the electron beam elongates in space (expansion velocity).



This is related to the type III duration at one frequency. However, it should be emphasized again that whilst velocity dispersion likely makes the most significant contribution toward the type III decay time, radio wave propagation effects, density turbulence and the radio emission process will also influence type III durations and derived speeds. As an example, Ratcliffe et al. (2014b) found that using the peak flux to estimate electron beam speeds from a dynamic spectrum of second harmonic emission, the derived exciter speed was more closely related to the region of the beam that produced the peak in back-scattered Langmuir waves, which was slightly farther back in space from where the peak Langmuir waves were generated.

When electron beams become unstable, it has been the focus of many recent theoretical works how density inhomogeneities in the background plasma influence subsequent Langmuir wave growth, electromagnetic emission and the development of the electron distribution function. Studies are typically carried out either in one spatial location (e.g., Ratcliffe and Kontar, 2014; Krafft et al., 2015; Voshchepynets and Krasnoselskikh, 2015; Voshchepynets et al., 2015), in a small spatial box (e.g., Thurgood and Tsiklauri, 2015; Volokitin and Krafft, 2018; Henri et al., 2019; Krafft and Volokitin, 2020) or over distance comparable to the solar corona or longer (e.g., Li et al., 2012; Reid and Kontar, 2013, 2015, 2017b; Loi et al., 2014; Ratcliffe et al., 2014b). Each of these different approaches has their own advantages and disadvantages and are used based upon the focus of the relevant study. Studies in one spatial location are computationally less expensive and are typically used to investigate how wave  $k$ -vectors develop over time, taking a static spatial gradient for the background density. Studies in a small spatial box focus on both on wave-particle and wave-wave interactions required to generate radio emission.

These studies aim for a more complete treatment of the problem, with the small spatial box and hence restrictive length scales necessary due to the computational overhead. Studies over large distances typically use the quasilinear approximation to reduce the computational overhead and try to capture the large-scale evolution of the beam-plasma system and the fine structure that occurs within the resulting Langmuir waves and radio waves that we detect as type III bursts.

It has been known for decades that density inhomogeneities in the background plasma suppress the generation of beam-induced Langmuir waves by refracting them in phase space, out of resonance with the electron beam. Langmuir waves refracted to low phase velocities (high  $k$ -vectors) are eventually re-absorbed by the background plasma. Langmuir waves refracted to high phase velocities can be re-absorbed by the electron beam, accelerating a tail of energetic electrons. The level of Langmuir wave suppression is dependent upon on the characteristic length scale of density inhomogeneities  $L \propto \frac{1}{n_e} \frac{\partial n_e}{\partial x}$  (e.g., Kontar, 2001; Reid and Kontar, 2010, 2017b; Voshchepynets et al., 2015; Krafft and Volokitin, 2020) such that if the magnitude of  $L$  reaches a certain value, Langmuir waves are suppressed. The level of density inhomogeneities also influence the conversion of Langmuir wave energy into electromagnetic energy (e.g., Li et al., 2012; Ratcliffe and Kontar, 2014; Krasnoselskikh et al., 2019).

When electric fields associated with Langmuir waves are measured in the solar wind at the same time as electron beams and type III bursts, they are distributed in spatial clumps (e.g., Vidojevic et al., 2012). This is attributed to aforementioned Langmuir wave suppression from density inhomogeneities. How the distribution of the beam-driven electric field is modified by density inhomogeneities has been simulated both locally

(Voshchepynets et al., 2017; Krafft and Volokitin, 2020), with an electron beam propagation through the solar corona and through the solar wind (Reid and Kontar, 2017b). Without any density fluctuations, the beam-driven electric field distribution is peaked at the highest electric fields. As the intensity of the density fluctuations increases, the logarithm of the electric field becomes more uniformly distributed and the mean field is decreased. When the intensity of the density fluctuations is high, the largest electric field amplitude part of the distribution is better approximated by a power-law or exponential decay. The effect was described probabilistically (Voshchepynets and Krasnoselskikh, 2015; Voshchepynets et al., 2015) and through resonance broadening (Bian et al., 2014). In the resonance broadening description, for homogeneous plasma, wave-particle interactions have a sharp resonance function  $\delta(\omega - kv)$ . For inhomogeneous plasma, wave particle interactions occur over a range of velocities  $\Delta v$  due to wave refraction and so the growth rate of the beam-plasma instability changes to become a function of the electron beam velocity gradient averaged over  $\Delta v$ . If this width is small then wave growth can still occur but as the width increases the average slope reduces and can even become positive (see **Figure 10**).

The most visible consequence of density inhomogeneities is the type IIIb radio burst fine structure which was discussed in section 3.1. Quasilinear simulations are able to capture the fluctuating Langmuir waves (e.g., Reid and Kontar, 2015) and produce dynamic spectra that are similar to type IIIb bursts (Li et al., 2012; Loi et al., 2014; Ratcliffe et al., 2014b). Indeed, without simulating density inhomogeneities the electron flux at 1 AU does not compare with *in situ* observations (Reid and Kontar, 2013). However, there are still notable discrepancies when comparing synthetic dynamic spectra to observations, particularly using recent high resolution imaging spectroscopy. Whilst the electric fields in the solar corona cannot currently be measured, for events that are also seen at lower frequencies, the *in situ* measurements of the beam-induced electric field from PSP and SoLO can be analyzed to see how they change as a function of distance from the Sun. Combining with numerical simulations, the measurements could be used to back-project the beam-induced electric field and infer what was happening in the solar corona, and then compared with the type III imaging spectroscopy of type IIIb striae bursts.

Many of the studies above use a 1D approximation for the propagation of electrons along magnetic field lines. Whilst this simplifies the models and is grounded by observations of electrons with small pitch angles at 1 AU, it is still a major simplification. Recent efforts have been undertaken (Ziebell et al., 2014, 2015, 2016; Tigik et al., 2016) to model the plasma emission process in two velocity dimensions for a single point in space, taking into account all the steps involved in the plasma emission process. In the simulations by Ziebell et al. (2015), fundamental emission was generated by Langmuir waves both with ion-sound waves and by scattering. These processes dominated initially, whilst over time the harmonic emission overtook the fundamental. Taking into account collisions, Tigik et al. (2016) found that a wider plateau was formed in the distribution function and increased the tendency to isotropization.

The bulk of the results documented above use the weak turbulence approximation to simulate electron beam dynamics. However, there has been significant effort to simulate the beam-plasma interaction and the subsequent generation of radio waves using the Zakharov equations (e.g., Zaslavsky et al., 2010; Krafft et al., 2015; Volokitin and Krafft, 2018; Krafft and Volokitin, 2020). This approach is not self-consistent with the electron beam exciter but has produced comparable type III fluxes using parameters in the solar wind. The plasma emission process has also been reproduced using particle-in-cell (PIC) codes (e.g., Thurgood and Tsiklauri, 2015; Henri et al., 2019). Both studies were able to produce electrostatic and electromagnetic waves through plasma instabilities. Henri et al. (2019) found weaker electron beams produced radio waves that were more forward directed at the source, whilst larger beam densities widened the Langmuir wave spectrum, leading to a larger available angular spread of radio emission. The validity of the weak turbulence approximation has been analyzed using PIC code both for 1D (Ratcliffe et al., 2014a) and 2D (Lee et al., 2019) weak turbulence codes. Both studies found a plateau forming in the beam region within comparable timescales, although the weak turbulence code developed a extended tail along the forward direction not seen in the PIC code (Lee et al., 2019). The Langmuir wave spectrum was similar unless the ion temperature was increased to the electron temperature or hotter (Ratcliffe et al., 2014a). In terms of radio emission Lee et al. (2019) found a good agreement, especially for larger beam velocities but it required a high number of particles per cell in the PIC codes.

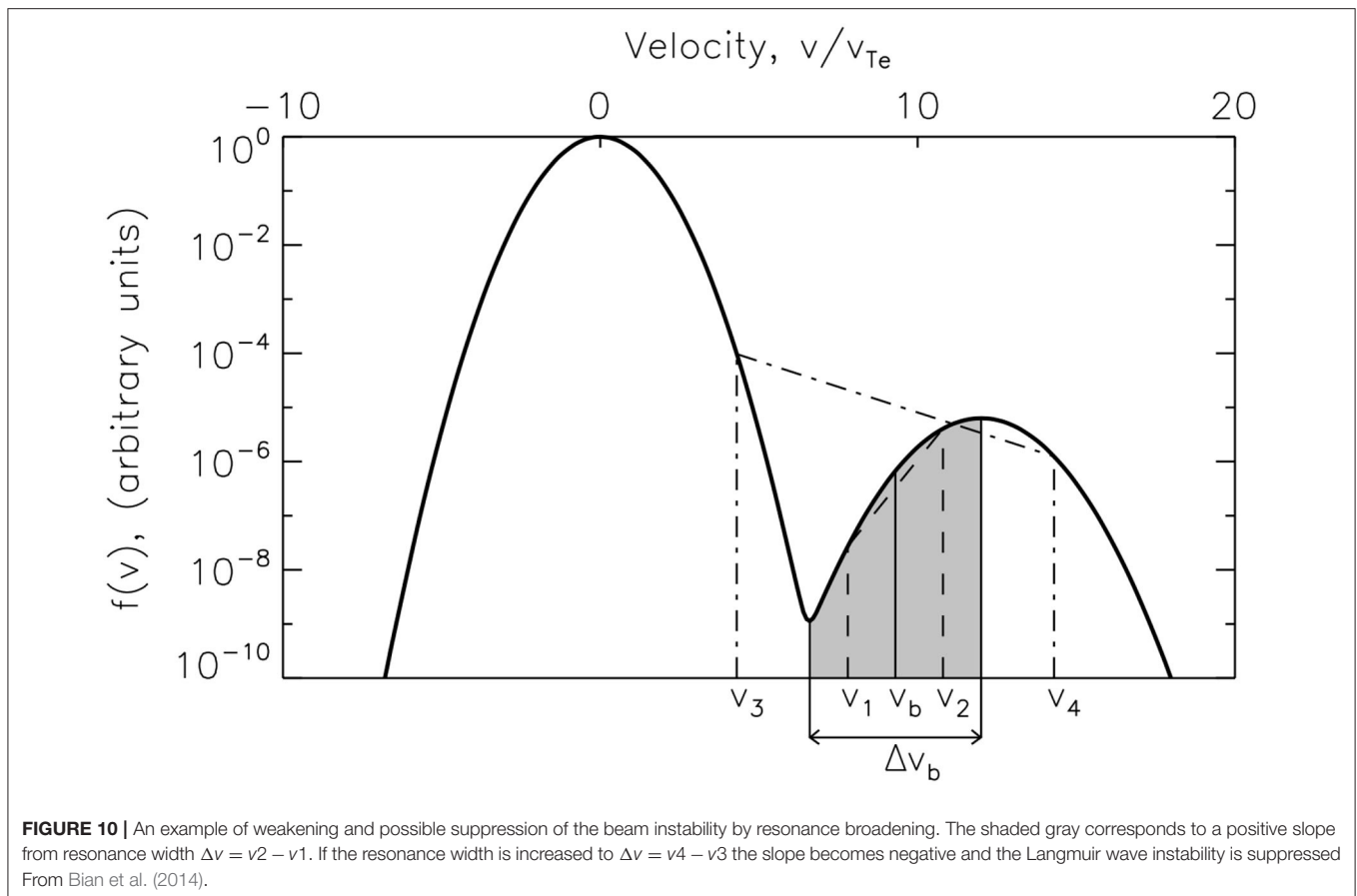
## 5. CONCLUSION

### 5.1. Future Observing

The future is bright for type III imaging spectroscopy. Not only are we now taking advantage of the capability of instruments like the VLA, MWA, and LOFAR but there are numerous new observational platforms that have either recently come online or will be operational very soon.

Starting at the ground, the first notable platform is the Mingantu Ultrawide Spectral Radioheliograph (MUSER, Yan et al., 2009, 2016), based in Inner Mongolia, China. Most relevant for type III bursts is MUSER I that will operate between 0.4 and 2 GHz. MUSER is a solar dedicated radio telescope unlike the astrophysical telescopes like LOFAR which means that it has a much higher chance of catching transient type III bursts when they occur and MUSER I has already observed a radio burst (Yan et al., 2016) around 1 GHz. MUSER I is poised to provide the community with a plethora of type III imaging spectroscopy data that will significantly help to understand the physics behind these radio bursts.

Another platform that will come online soon is the Square Kilometer Array (SKA, see Nindos et al., 2019, for a solar physics overview). Both the SKA1-LOW, observing between 50 and 350 MHz and the SKA1-MID, observing from 0.35 to 15.3 GHz will be relevant for observing type III bursts from different regions within the solar corona. Commissioning of SKA1 is expected to start in 2024. With SKA1-LOW being based in Western Australia it should hopefully be available to pair with



MUSER I for complimentary observations of type III imaging spectroscopy from the low to high corona. Similarly, SKA1-MID is based in the Karoo desert of South Africa and should be able to take complimentary type III observations with LOFAR. Both the sensitivity and angular resolution of SKA will be much better than what has come before and promises to provide major advances on key type III science questions.

Going into space and the launch of Parker Solar Probe and Solar Orbiter has far-reaching implications for type III theory. Both spacecraft are spectroscopically observing type III bursts from 20 MHz and below from changing vantage points around the solar system. They are also taking *in situ* particle measurements at different distances from the Sun that will allow analysis of high energy electrons, solar wind particles and plasma waves. ESAs BepiColombo should provide a third point in the inner solar wind for radio wave and *in situ* plasma measurements when the Mio spacecraft starts science operations.

On the horizon are two NASA space missions that are attempting to break the 10 MHz frequency barrier for type III imaging spectroscopy. CURIE (Sundkvist et al., 2016) is a two-cubesat mission that will formation fly in low-Earth orbit with a few km separation. It will take imaging spectroscopy observations of the Sun from 40 to 0.1 MHz. SunRISE (Alibay et al., 2017) is a six-cubesat mission that will fly slightly above the Geostationary Equatorial Orbit in a passive formation that

will allow the formation of an interferometer whilst minimizing operations complexity. SunRISE will take imaging spectroscopy observations of the Sun from 25 to 0.1 MHz. Both missions intend to observe type III bursts. A further mission concept study NOIRE (Ceccconi et al., 2018) is being developed in Europe to launch a swarm of nanosatellites for imaging low frequency radio emission targetted toward the astronomical dark ages and planetary radio emissions. Such a venture would certainly be of use for observing type III bursts.

## 5.2. Outstanding Science Questions

Our new age of type III imaging spectroscopy has already brought us many new observational discoveries. The high frequency VLA observations are showing us the signatures of energetic particles very close to their acceleration site. Low frequency MWA and LOFAR observations are showing us how the particles are escaping the Sun and what the structure of the upper corona is like. However, there are still many challenging science questions that require detailed answers, which type III imaging spectroscopy can help contribute.

*Where are the locations of electron acceleration sites and what physical processes accelerate electrons?* Electron acceleration properties are generally assumed in type III studies and not self-consistently generated by an acceleration mechanism. There are a few works done in the context of 3D magnetic reconnection,

based on particle-in-cell codes, that focus on the physical mechanisms behind electron acceleration at reconnection sites (e.g., Markidis et al., 2013). Type IIIs regularly appear in groups which is not traditionally simulated, nor the duration of these groups fully understood. As indicated in section 2, we have started to address these issues with the help of high frequency type IIIs (e.g., Chen B. et al., 2018) and combined analysis with other wavelengths (e.g., Reid et al., 2014) but there still remains significant uncertainty on the spatial characteristics of acceleration sites. For example, are all electron beams that make type III groups accelerated in a compact volume, or spread throughout a larger volume around 1,000 Mm<sup>3</sup>? Do they change location in time? Is there size connected with type III burst properties? Type III analysis has provided observational constraints on accelerated electron beam parameters such as characteristic times and electron energies. Electron acceleration can certainly occur at a range of heights in the solar corona, with high frequency type III bursts starting low in the corona and type III noise storm sources probably being accelerated much higher in the corona. Does the same acceleration mechanism produce electron beams that form type III bursts at 10 and 200 Mm? Type III imaging spectroscopy will help by catching the location of the type III starting frequency and the subsequent evolution of position in time. It will also allow the localization of acceleration through the imaging of bi-directional type III bursts.

*What physical processes are responsible for the transport of accelerated electrons?* Whilst we have a general understanding of how wave-particle interactions affect the propagation of electrons through the solar atmosphere (e.g., Reid and Kontar, 2018b), there are still unknowns about how the 3D phase space properties of these particle beams evolves with time as they propagate away from the acceleration region. Recent numerical studies are not taking into account modeling large spatial scales in three dimensions and we risk missing many details (Harding et al., 2020), in a similar way that 3D magnetic reconnection is different from 2D. Type III imaging spectroscopy has been helping to answer this question about electron transport by analyzing the spatial evolution of different frequencies with time (e.g., Zhang et al., 2019). Such studies can confirm and constrain numerical simulations, with the imaging spectroscopy providing more detailed diagnostics about the spatial location of electron beams with time as they travel out through the solar corona. These studies are only just beginning and there is still much to be analyzed both statistically and using single event studies. The combination of electron beam diagnostics from type III imaging spectroscopy studies with *in situ* measurements from PSP and SolO should provide significant clarity on how electron beams evolve through the solar system and help disentangle transport and acceleration effects.

*How does the type III emission mechanism influence observed properties?* There are still many open questions about how Langmuir waves undergo wave-wave coupling to produce radio waves, and when fundamental emission dominates over harmonic emission. Analysis of type III fine structures should help answer this question and is an area of type III study that is significantly enhanced by new imaging spectroscopy.

There has already been notable advances in the evolution of type III striae (e.g., Sharykin et al., 2018) that are providing us with new insight on small-scale dynamics. Imaging spectroscopy analysis of the location and spatial extent between fundamental and harmonic emission (e.g., Kontar et al., 2017) have been providing observational constraints that can help develop theoretical models (e.g., Li and Cairns, 2013; Ratcliffe et al., 2014b; Krasnoselskikh et al., 2019) that are describing these non-linear processes. Future imaging spectroscopy should be used to further analyse fundamental and harmonic image properties as a function of frequency as their differences diagnose how the distinct wave-wave processes modify the radio burst properties, provided light transport effects are accounted for.

*What properties are intrinsic to the type III source and what are caused by light transport effects?* There has been a reinvigorated effort recently to understand and model how radio waves travel from the solar corona to Earth. It is apparent that the scattering of waves off density fluctuations significantly affect what we observe at Earth, in particular for low frequency fundamental emission. If we want to fully unlock the benefits of type III imaging spectroscopy we must be able to untangle these effects and significant efforts are already under way (e.g., Kontar et al., 2019). The variation in source parameters as a function of frequency can be used to constrain and improve the ray-tracing models that are being used to describe light transport. However, as with many complex processes, knowledge of light scattering can, and is, providing new diagnostics of the turbulent nature of the solar corona.

*What is the structure of the flaring solar corona?* Type III studies have been approximating the density structure of the solar corona for some time and directly producing a number of density models (e.g., Cairns et al., 2009; Saint-Hilaire et al., 2013). As discussed in section 3, the validity of these and other density models is something that is being tested by current observations using type IIIs for magnetic loops that extend into the solar wind (e.g., McCauley et al., 2018) and using U-burst observations for magnetic loops confined to the corona (e.g., Reid and Kontar, 2017a). Imaging radio sources at coronal heights around 1 solar radii and above will help to understand the structure of the magnetic field as it evolves from the corona to the solar wind. Despite this, our estimates of source heights are still uncertain and we are yet to have a good handle on source projection effects, something that is likely to elude us without some future mission that can perform radio interferometric imaging from a spacecraft not near the Earth.

To help answer the above science questions, we must overcome a number of logistical challenges we face in the coming years. The advent of high volume data sets will bring with it significant challenges to store and analyse such large amounts of data. The astrophysical telescopes that are providing some of the new high resolution type III imaging spectroscopy are only observing the Sun sporadically. Whilst there has been numerous successful observing campaigns already on all these telescopes, the limited observing time will miss most type III radio bursts and highlights the benefits of solar monitoring for capturing type

III burst activity from the Sun. Additionally the solar coverage in radio frequencies is not uniform around the globe and we risk missing key information when the Sun provides us with interesting type III events.

What is certain is that our new radio interferometer tools are allowing type III imaging spectroscopy with much higher spatial, spectral and temporal resolution than ever before. Not only are we going to further our understanding of the science questions described above, this new leap in solar radio observing is likely to bring about new discoveries that we have not even thought of yet. Furthering our quest to enable type III bursts as remote sensors of astrophysical plasma.

## REFERENCES

- Alibay, F., Kasper, J. C., Lazio, T. J. W., and Neilsen, T. (2017). "Sun radio interferometer space experiment (SunRISE): tracking particle acceleration and transport in the inner heliosphere," in *2017 IEEE Aerospace Conference* (Big Sky, MT), 1–15. doi: 10.1109/AERO.2017.7943789
- Allen, C. W. (1947). Interpretation of electron densities from corona brightness. *Monthly Notices R. Astron. Soc.* 107:426. doi: 10.1093/mnras/107.5-6.426
- Alvarez, H., and Haddock, F. T. (1973). Solar wind density model from km-wave type III bursts. *Sol. Phys.* 29, 197–209. doi: 10.1007/BF00153449
- Arzner, K., and Benz, A. O. (2005). Temporal correlation of hard x-rays and meter/decimeter radio structures in solar flares. *Sol. Phys.* 231, 117–141. doi: 10.1007/s11207-005-1590-8
- Arzner, K., and Magun, A. (1999). Radiowave propagation in a statistically inhomogeneous plasma. *Astron. Astrophys.* 351, 1165–1189.
- Aschwanden, M. J., and Benz, A. O. (1997). Electron densities in solar flare loops, chromospheric evaporation upflows, and acceleration sites. *Astrophys. J.* 480, 825–839. doi: 10.1086/303995
- Aschwanden, M. J., Montello, M. L., Dennis, B. R., and Benz, A. O. (1995). Sequences of correlated hard X-ray and type III bursts during solar flares. *Astrophys. J.* 440, 394–406. doi: 10.1086/175281
- Aubier, M., and Boischoat, A. (1972). Exciter of type III bursts and coronal temperature. *Astron. Astrophys.* 19:343–353.
- Bain, H. M., and Fletcher, L. (2009). Hard X-ray emission from a flare-related jet. *Astron. Astrophys.* 508, 1443–1452. doi: 10.1051/0004-6361/200911876
- Barrow, C. H., and Achong, A. (1975). Solar type III burst profiles at decametre-wave frequencies. I - Observations. II - Exciter. *Sol. Phys.* 45, 459–465. doi: 10.1007/BF00158462
- Bastian, T. S. (1990). Radio emission from flare stars. *Sol. Phys.* 130, 265–294. doi: 10.1007/BF00156794
- Bian, N. H., Emslie, A. G., and Kontar, E. P. (2019). A Fokker-Planck framework for studying the diffusion of radio burst waves in the solar corona. *Astrophys. J.* 873:33. doi: 10.3847/1538-4357/ab0411
- Bian, N. H., Kontar, E. P., and Ratcliffe, H. (2014). Resonance broadening due to particle scattering and mode coupling in the quasi-linear relaxation of electron beams. *J. Geophys. Res.* 119, 4239–4255. doi: 10.1002/2013JA019664
- Bisoi, S. K., Sawant, H. S., Janardhan, P., Yan, Y., Chen, L., Awasthi, A. K., et al. (2018). Decimetric emission 500 arcsecs away from a flaring site: possible scenarios from GMRT solar radio observations. *Astrophys. J.* 862:65. doi: 10.3847/1538-4357/aacd07
- Cairns, I. H., Lobzin, V. V., Donea, A., Tingay, S. J., McCauley, P. I., Oberoi, D., et al. (2018). Low altitude solar magnetic reconnection, type III solar radio bursts, and x-ray emissions. *Sci. Rep.* 8:1676. doi: 10.1038/s41598-018-19195-3
- Cairns, I. H., Lobzin, V. V., Warmuth, A., Li, B., Robinson, P. A., and Mann, G. (2009). Direct radio probing and interpretation of the sun's plasma density profile. *Astrophys. J. Lett.* 706, L265–L269. doi: 10.1088/0004-637X/706/2/L265
- Carley, E. P., Vilmer, N., and Gallagher, P. T. (2016). Radio diagnostics of electron acceleration sites during the eruption of a flux rope in the solar corona. *Astrophys. J.* 833:87. doi: 10.3847/1538-4357/833/1/87

## AUTHOR CONTRIBUTIONS

HR contributed all of the text to the document.

## ACKNOWLEDGMENTS

I want to acknowledge all the authors that produced the high-quality research which was reviewed in this article. I also want to acknowledge the support that goes into running the many ground-based radio observatories that provided the data for these studies. Finally I want to acknowledge the helpful and interesting discussions about type III bursts with by colleagues over the years.

- Cecconi, B., Dekkali, M., Briand, C., Segret, B., Girard, J. N., Laurens, A., et al. (2018). "NOIRE study report: towards a low frequency radio interferometer in space," in *2018 IEEE Aerospace Conference* (Big Sky, MT), 1–19. doi: 10.1109/AERO.2018.8396742
- Chen, B., Bastian, T. S., White, S. M., Gary, D. E., Perley, R., Rupen, M., et al. (2013). Tracing electron beams in the sun's corona with radio dynamic imaging spectroscopy. *Astrophys. J. Lett.* 763:L21. doi: 10.1088/2041-8205/763/1/L21
- Chen, B., Yu, S., Battaglia, M., Farid, S., Savcheva, A., Reeves, K. K., et al. (2018). Magnetic reconnection null points as the origin of semirelativistic electron beams in a solar jet. *Astrophys. J.* 866:62. doi: 10.3847/1538-4357/aadb89
- Chen, C. H. K. (2016). Recent progress in astrophysical plasma turbulence from solar wind observations. *J. Plasma Phys.* 82:535820602. doi: 10.1017/S0022377816001124
- Chen, X., Kontar, E. P., Yu, S., Yan, Y., Huang, J., and Tan, B. (2018). Fine structures of solar radio type III bursts and their possible relationship with coronal density turbulence. *Astrophys. J.* 856:73. doi: 10.3847/1538-4357/aaa9bf
- Chrysaphi, N., Kontar, E. P., Holman, G. D., and Temmer, M. (2018). CME-driven shock and type II solar radio burst band splitting. *Astrophys. J.* 868:79. doi: 10.3847/1538-4357/aae9e5
- de La Noe, J., and Boischoat, A. (1972). The type III B burst. *Astron. Astrophys.* , 20:55.
- Drake, J. F., Swisdak, M., Che, H., and Shay, M. A. (2006). Electron acceleration from contracting magnetic islands during reconnection. *Nature* 443, 553–556. doi: 10.1038/nature05116
- Dulk, G. A. (1985). Radio emission from the sun and stars. *Annu. Rev. Astron. Astrophys.* 23, 169–224. doi: 10.1146/annurev.aa.23.090185.001125
- Ellingson, S. W., Clarke, T. E., Cohen, A., Craig, J., Kassim, N. E., Pihlstrom, Y., et al. (2009). The long wavelength array. *IEEE Proc.* 97, 1421–1430. doi: 10.1109/JPROC.2009.2015683
- Feng, S. W., Chen, Y., Song, H. Q., Wang, B., and Kong, X. L. (2016). An imaging study of a complex solar coronal radio eruption. *Astrophys. J. Lett.* 827:L9. doi: 10.3847/2041-8205/827/1/L9
- Fox, N. J., Velli, M. C., Bale, S. D., Decker, R., Driesman, A., Howard, R. A., et al. (2016). The solar probe plus mission: humanity's first visit to our star. *Space Sci. Rev.* 204, 7–48. doi: 10.1007/s11214-015-0211-6
- Gary, D. E., Bastian, T. S., Chen, B., Fleishman, G. D., and Glesener, L. (2018). "Radio observations of solar flares," in *Astronomical Society of the Pacific Conference Series*, 99.
- Gibson, S., Kucera, T., White, S., Dove, J., Fan, Y., Forland, B., et al. (2016). FORWARD: a toolset for multiwavelength coronal magnetometry. *Front. Astron. Space Sci.* 3:8. doi: 10.3389/fspas.2016.00008
- Gordovskyy, M., Kontar, E., Browning, P., and Kuznetsov, A. (2019). Frequency-distance structure of solar radio sources observed by LOFAR. *Astrophys. J.* 873:48. doi: 10.3847/1538-4357/ab03d8
- Hamilton, R. J., Petrosian, V., and Benz, A. O. (1990). Statistical study of the correlation of hard X-ray and type III radio bursts in solar flares. *Astrophys. J.* 358, 644–653. doi: 10.1086/169017
- Harding, J. C., Cairns, I. H., and Melrose, D. B. (2020). Electron-Langmuir wave resonance in three dimensions. *Phys. Plasmas* 27:020702. doi: 10.1063/1.5139068

- Henri, P., Sgattoni, A., Briand, C., Amiranoff, F., and Riconda, C. (2019). Electromagnetic simulations of solar radio emissions. *J. Geophys. Res.* 124, 1475–1490. doi: 10.1029/2018JA025707
- Holman, G. D., Aschwanden, M. J., Aurass, H., Battaglia, M., Grigis, P. C., Kontar, E. P., et al. (2011). Implications of x-ray observations for electron acceleration and propagation in solar flares. *Space Sci. Rev.* 159, 107–166. doi: 10.1007/978-1-4614-3073-5\_4
- Islaker, H., and Benz, A. O. (1994). Catalogue of 1–3 GHz solar flare radio emission. *Astron. Astrophys. Suppl. Ser.* 104, 145–160.
- Kane, S. R. (1972). Evidence for a common origin of the electrons responsible for the impulsive x-ray and type III radio bursts. *Sol. Phys.* 27, 174–181. doi: 10.1007/BF00151781
- Kane, S. R., Benz, A. O., and Treumann, R. A. (1982). Electron acceleration in impulsive solar flares. *Astrophys. J.* 263, 423–432. doi: 10.1086/160514
- Kerdran, A., and Delouis, J.-M. (1997). “The Nançay radioheliograph,” in *Coronal Physics from Radio and Space Observations*, ed G. Trotter (Berlin: Springer Verlag), 192. doi: 10.1007/BF0106458
- Kishore, P., Kathiravan, C., Ramesh, R., Rajalingam, M., and Barve, I. V. (2014). Gauribidanur low-frequency solar spectrograph. *Sol. Phys.* 289, 3995–4005. doi: 10.1007/s11207-014-0539-1
- Klassen, A., Gómez-Herrero, R., and Heber, B. (2011). Electron spikes, type III radio bursts and EUV jets on 22 February 2010. *Sol. Phys.* 273, 413–419. doi: 10.1007/s11207-011-9735-4
- Kolotkov, D. Y., Nakariakov, V. M., and Kontar, E. P. (2018). Origin of the modulation of the radio emission from the solar corona by a fast magnetoacoustic wave. *Astrophys. J.* 861:33. doi: 10.3847/1538-4357/aac77e
- Kong, X., Chen, Y., Feng, S., Du, G., Li, C., Koval, A., et al. (2016). Observation of a metric type N solar radio burst. *Astrophys. J.* 830:37. doi: 10.3847/0004-637X/830/1/37
- Konovalenko, A., Sodin, L., Zakharenko, V., Zarka, P., Ulyanov, O., Sidorchuk, M., et al. (2016). The modern radio astronomy network in Ukraine: UTR-2, URAN and GURT. *Exp. Astron.* 42, 11–48. doi: 10.1007/s10686-016-9498-x
- Kontar, E. P. (2001). Dynamics of electron beams in the inhomogeneous solar corona plasma. *Sol. Phys.* 202, 131–149. doi: 10.1023/A:1011894830942
- Kontar, E. P., Brown, J. C., Emslie, A. G., Hajdas, W., Holman, G. D., Hurford, G. J., et al. (2011). Deducing electron properties from hard x-ray observations. *Space Sci. Rev.* 159, 301–355. doi: 10.1007/978-1-4614-3073-5\_8
- Kontar, E. P., Chen, X., Chrysaphi, N., Jeffrey, N. L. S., Emslie, A. G., Krupar, V., et al. (2019). Anisotropic radio-wave scattering and the interpretation of solar radio emission observations. *Astrophys. J.* 884:122. doi: 10.3847/1538-4357/ab40bb
- Kontar, E. P., Lapshin, V. I., and Mel’Nik, V. N. (1998). Numerical and analytical study of the propagation of a monoenergetic electron beam in a plasma. *Plasma Phys. Rep.* 24, 772–776.
- Kontar, E. P., Yu, S., Kuznetsov, A. A., Emslie, A. G., Alcock, B., Jeffrey, N. L. S., et al. (2017). Imaging spectroscopy of solar radio burst fine structures. *Nat. Commun.* 8:1515. doi: 10.1038/s41467-017-01307-8
- Krafft, C., and Volokitin, A. S. (2020). Electromagnetic radiation from upper-hybrid wave turbulence in inhomogeneous solar plasmas. *Plasma Phys. Controlled Fusion* 62:024007. doi: 10.1088/1361-6587/ab569d
- Krafft, C., Volokitin, A. S., and Krasnoselskikh, V. V. (2015). Langmuir wave decay in inhomogeneous solar wind plasmas: simulation results. *Astrophys. J.* 809:176. doi: 10.1088/0004-637X/809/2/176
- Krasnoselskikh, V., Voshchepynets, A., and Maksimovic, M. (2019). On the efficiency of the linear-mode conversion for generation of solar type III radio bursts. *Astrophys. J.* 879:51. doi: 10.3847/1538-4357/ab22bf
- Krucker, S., Kontar, E. P., Christe, S., Glesener, L., and Lin, R. P. (2011). Electron acceleration associated with solar jets. *Astrophys. J.* 742:82. doi: 10.1088/0004-637X/742/2/82
- Krupar, V., Maksimovic, M., Kontar, E. P., Zaslavsky, A., Santolik, O., Soucek, J., et al. (2018). Interplanetary type III bursts and electron density fluctuations in the solar wind. *Astrophys. J.* 857:82. doi: 10.3847/1538-4357/aab60f
- Krupar, V., Szabo, A., Maksimovic, M., Kruparova, O., Kontar, E. P., Balmaceda, L. A., et al. (2020). Density fluctuations in the solar wind based on type III radio bursts observed by parker solar probe. *Astrophys. J. Suppl. Ser.* 246:57. doi: 10.3847/1538-4365/ab65bd
- Kundu, M. R., Gergely, T. E., Turner, P. J., and Howard, R. A. (1983). Direct evidence of type III electron streams propagating in coronal streamers. *Astrophys. J. Lett.* 269, L67–L71. doi: 10.1086/184057
- Leblanc, Y., and de La Noe, J. (1977). Solar radio type III bursts and coronal density structures. *Sol. Phys.* 52, 133–139. doi: 10.1007/BF00935796
- Lecacheux, A. (2000). *The Nançay Decameter Array: A Useful Step Towards Giant, New Generation Radio Telescopes for Long Wavelength Radio Astronomy*. Washington, DC” American Geophysical Union Geophysical Monograph Series. doi: 10.1029/GM119p0321
- Lee, S.-Y., Ziebell, L. F., Yoon, P. H., Gaelzer, R., and Lee, E. S. (2019). Particle-in-cell and weak turbulence simulations of plasma emission. *Astrophys. J.* 871:74. doi: 10.3847/1538-4357/aaf476
- Li, B., and Cairns, I. H. (2013). Type III bursts produced by power law injected electrons in Maxwellian background coronal plasmas. *J. Geophys. Res.* 118, 4748–4759. doi: 10.1002/jgra.50445
- Li, B., and Cairns, I. H. (2014). Fundamental emission of type III bursts produced in non-Maxwellian coronal plasmas with kappa-distributed background particles. *Sol. Phys.* 289, 951–976. doi: 10.1007/s11207-013-0375-8
- Li, B., Cairns, I. H., and Robinson, P. A. (2012). Frequency fine structures of type III bursts due to localized medium-scale density structures along paths of type III beams. *Sol. Phys.* 279, 173–196. doi: 10.1007/s11207-012-0001-1
- Li, B., Cairns, I. H., Yan, Y. H., and Robinson, P. A. (2011). Decimetric type III bursts: generation and propagation. *Astrophys. J. Lett.* 738:L9. doi: 10.1088/2041-8205/738/1/L9
- Lionello, R., Linker, J. A., and Mikić, Z. (2009). Multispectral emission of the sun during the first whole sun month: magnetohydrodynamic simulations. *Astrophys. J.* 690, 902–912. doi: 10.1088/0004-637X/690/1/902
- Loi, S. T., Cairns, I. H., and Li, B. (2014). Production of fine structures in type III solar radio bursts due to turbulent density profiles. *Astrophys. J.* 790:67. doi: 10.1088/0004-637X/790/1/67
- Lonsdale, C. J., Cappallo, R. J., Morales, M. F., Briggs, F. H., Benkevitch, L., Bowman, J. D., et al. (2009). The murchison widefield array: design overview. *IEEE Proc.* 97, 1497–1506. doi: 10.1109/JPROC.2009.2017564
- Magelssen, G. R., and Smith, D. F. (1977). Nonrelativistic electron stream propagation in the solar atmosphere and type III radio bursts. *Sol. Phys.* 55, 211–240. doi: 10.1007/BF00150886
- Mann, G., Bretiling, F., Vocks, C., Aurass, H., Steinmetz, M., Strassmeier, K. G., et al. (2018). Tracking of an electron beam through the solar corona with LOFAR. *Astron. Astrophys.* 611:A57. doi: 10.1051/0004-6361/201629017
- Markidis, S., Henri, P., Lapenta, G., Divin, A., Goldman, M., Newman, D., et al. (2013). Kinetic simulations of plasmoid chain dynamics. *Phys. Plasmas* 20:082105. doi: 10.1063/1.4817286
- Maxwell, A., and Swarup, G. (1958). A new spectral characteristic in solar radio emission. *Nature* 181, 36–38. doi: 10.1038/181036a0
- McCauley, P. I., Cairns, I. H., and Morgan, J. (2018). Densities probed by coronal type III radio burst imaging. *Sol. Phys.* 293:132. doi: 10.1007/s11207-018-1353-y
- McCauley, P. I., Cairns, I. H., Morgan, J., Gibson, S. E., Harding, J. C., Lonsdale, C., et al. (2017). Type III solar radio burst source region splitting due to a quasi-separatrix layer. *Astrophys. J.* 851:151. doi: 10.3847/1538-4357/aa9cee
- McLean, D. J., and Labrum, N. R. (1985). *Solar Radiophysics: Studies of Emission from the Sun at Metre Wavelengths*. Cambridge University Press.
- Mel’Nik, V. N. (1995). “Gas-dynamic” expansion of a fast-electron flux in a plasma. *Plasma Phys. Rep.* 21, 89–91.
- Mel’Nik, V. N., Konovalenko, A. A., Rucker, H. O., Boiko, A. I., Dorovskyy, V. V., Abranin, E. P., et al. (2011). Observations of powerful type III bursts in the frequency range 10–30 MHz. *Sol. Phys.* 269, 335–350. doi: 10.1007/s11207-010-9703-4
- Mel’Nik, V. N., Lapshin, V., and Kontar, E. (1999). Propagation of a monoenergetic electron beam in the solar corona. *Sol. Phys.* 184, 353–362. doi: 10.1023/A:1005191910544
- Mohan, A., Mondal, S., Oberoi, D., and Lonsdale, C. J. (2019). Evidence for super-Alfvénic oscillations in solar type III radio burst sources. *Astrophys. J.* 875:98. doi: 10.3847/1538-4357/ab0ae5
- Mohan, A., and Oberoi, D. (2017). 4D data cubes from radio-interferometric spectroscopic snapshot imaging. *Sol. Phys.* 292:168. doi: 10.1007/s11207-017-1193-1
- Morosan, D. E., and Gallagher, P. T. (2017). “Characteristics of type III radio bursts and solar S bursts,” in *Planetary Radio Emissions VIII*, eds G. Fischer, G. Mann,

- M. Panchenko, and P. Zarka (Vienna: Austrian Academy of Sciences Press), 357–368.
- Morosan, D. E., Gallagher, P. T., Fallows, R. A., Reid, H., Mann, G., Bisi, M. M., et al. (2017). The association of a J-burst with a solar jet. *Astron. Astrophys.* 606:A81. doi: 10.1051/0004-6361/201629996
- Morosan, D. E., Gallagher, P. T., Zucca, P., Fallows, R., Carley, E. P., Mann, G., et al. (2014). LOFAR tied-array imaging of Type III solar radio bursts. *Astron. Astrophys.* 568:A67. doi: 10.1051/0004-6361/201423936
- Morosan, D. E., Gallagher, P. T., Zucca, P., O'Flannagain, A., Fallows, R., Reid, H., et al. (2015). LOFAR tied-array imaging and spectroscopy of solar S bursts. *Astron. Astrophys.* 580:A65. doi: 10.1051/0004-6361/201526064
- Mugundhan, V., Hariharan, K., and Ramesh, R. (2017). Solar type IIIb radio bursts as tracers for electron density fluctuations in the corona. *Sol. Phys.* 292:155. doi: 10.1007/s11207-017-1181-5
- Mulay, S. M., Sharma, R., Valori, G., Vásquez, A. M., Del Zanna, G., Mason, H., et al. (2019). Study of the spatial association between an active region jet and a nonthermal type III radio burst. *Astron. Astrophys.* 632:A108. doi: 10.1051/0004-6361/201936369
- Müller, D., Marsden, R. G., St. Cyr, O. C., and Gilbert, H. R. (2013). Solar orbiter. Exploring the sun-heliosphere connection. *Sol. Phys.* 285, 25–70. doi: 10.1007/s11207-012-0085-7
- Newkirk, G. Jr. (1961). The solar corona in active regions and the thermal origin of the slowly varying component of solar radio radiation. *Astrophys. J.* 133:983. doi: 10.1086/147104
- Nindos, A., Kontar, E. P., and Oberoi, D. (2019). Solar physics with the square kilometre array. *Adv. Space Res.* 63, 1404–1424. doi: 10.1016/j.asr.2018.10.023
- Payne-Scott, R., Yabsley, D. E., and Bolton, J. G. (1947). Relative times of arrival of bursts of solar noise on different radio frequencies. *Nature* 160, 256–257. doi: 10.1038/160256b0
- Perley, R. A., Chandler, C. J., Butler, B. J., and Wrobel, J. M. (2011). The expanded very large array: a new telescope for new science. *Astrophys. J. Lett.* 739:L1. doi: 10.1088/2041-8205/739/1/L1
- Pick, M., and Vilmer, N. (2008). Sixty-five years of solar radioastronomy: flares, coronal mass ejections and Sun Earth connection. *Astron. Astrophys. Rev.* 16, 1–153. doi: 10.1007/s00159-008-0013-x
- Rahman, M. M., Cairns, I. H., and McCauley, P. I. (2020). Spectropolarimetric imaging of metric type III solar radio bursts. *Sol. Phys.* 295:51. doi: 10.1007/s11207-020-01616-0
- Ratcliffe, H., Brady, C. S., Che Rozenan, M. B., and Nakariakov, V. M. (2014a). A comparison of weak-turbulence and particle-in-cell simulations of weak electron-beam plasma interaction. *Phys. Plasmas* 21:122104. doi: 10.1063/1.4904065
- Ratcliffe, H., and Kontar, E. P. (2014). Plasma radio emission from inhomogeneous collisional plasma of a flaring loop. *Astron. Astrophys.* 562:A57. doi: 10.1051/0004-6361/201322263
- Ratcliffe, H., Kontar, E. P., and Reid, H. A. S. (2014b). Large-scale simulations of solar type III radio bursts: flux density, drift rate, duration, and bandwidth. *Astron. Astrophys.* 572:A111. doi: 10.1051/0004-6361/201423731
- Reid, H. A. S. (2016). *Solar Type III Bursts Observed with LOFAR*. URSI Asia-Pacific Radio Science Conference (URSI AP-RASC). doi: 10.1109/URSIAP-RASC.2016.7601384
- Reid, H. A. S., and Kontar, E. P. (2010). Solar wind density turbulence and solar flare electron transport from the Sun to the Earth. *Astrophys. J.* 721, 864–874. doi: 10.1088/0004-637X/721/1/864
- Reid, H. A. S., and Kontar, E. P. (2013). Evolution of the solar flare energetic electrons in the inhomogeneous inner heliosphere. *Sol. Phys.* 285, 217–232. doi: 10.1007/s11207-012-0013-x
- Reid, H. A. S., and Kontar, E. P. (2015). Stopping frequency of type III solar radio bursts in expanding magnetic flux tubes. *Astron. Astrophys.* 577:A124. doi: 10.1051/0004-6361/201425309
- Reid, H. A. S., and Kontar, E. P. (2017a). Imaging spectroscopy of type U and J solar radio bursts with LOFAR. *Astron. Astrophys.* 606:A141. doi: 10.1051/0004-6361/201730701
- Reid, H. A. S., and Kontar, E. P. (2017b). Langmuir wave electric fields induced by electron beams in the heliosphere. *Astron. Astrophys.* 598:A44. doi: 10.1051/0004-6361/201629697
- Reid, H. A. S., and Kontar, E. P. (2018a). Solar type III radio burst time characteristics at LOFAR frequencies and the implications for electron beam transport. *Astron. Astrophys.* 614:A69. doi: 10.1051/0004-6361/201732298
- Reid, H. A. S., and Kontar, E. P. (2018b). Spatial expansion and speeds of type III electron beam sources in the solar corona. *Astrophys. J.* 867:158. doi: 10.3847/1538-4357/aae5d4
- Reid, H. A. S., and Ratcliffe, H. (2014). A review of solar type III radio bursts. *Res. Astron. Astrophys.* 14, 773–804. doi: 10.1088/1674-4527/14/7/003
- Reid, H. A. S., and Vilmer, N. (2017). Coronal type III radio bursts and their X-ray flare and interplanetary type III counterparts. *Astron. Astrophys.* 597:A77. doi: 10.1051/0004-6361/201527758
- Reid, H. A. S., Vilmer, N., and Kontar, E. P. (2011). Characteristics of the flare acceleration region derived from simultaneous hard X-ray and radio observations. *Astron. Astrophys.* 529:A66. doi: 10.1051/0004-6361/201016181
- Reid, H. A. S., Vilmer, N., and Kontar, E. P. (2014). The low-high-low trend of type III radio burst starting frequencies and solar flare hard X-rays. *Astron. Astrophys.* 567:A85. doi: 10.1051/0004-6361/201321973
- Riddle, A. C. (1974). On the Determination of coronal temperature from the decay of type III radio bursts. *Sol. Phys.* 34, 181–184. doi: 10.1007/BF00149609
- Robinson, R. D. (1983). Scattering of radio waves in the solar corona. *Proc. Astron. Soc. Austral.* 5, 208–211. doi: 10.1017/S132335800001688X
- Roelof, E. C., and Pick, M. (1989). Type III radio bursts in a fibrous corona. *Astron. Astrophys.* 210, 417–424.
- Saint-Hilaire, P., Vilmer, N., and Kerdran, A. (2013). A decade of solar type III radio bursts observed by the Nançay radioheliograph 1998–2008. *Astrophys. J.* 762:60. doi: 10.1088/0004-637X/762/1/60
- Saito, K., Poland, A. I., and Munro, R. H. (1977). A study of the background corona near solar minimum. *Sol. Phys.* 55, 121–134. doi: 10.1007/BF00150879
- Schrijver, C. J., Sandman, A. W., Aschwanden, M. J., and De Rosa, M. L. (2004). The coronal heating mechanism as identified by full-sun visualizations. *Astrophys. J.* 615, 512–525. doi: 10.1086/424028
- Sharykin, I. N., Kontar, E. P., and Kuznetsov, A. A. (2018). LOFAR observations of fine spectral structure dynamics in type IIIb radio bursts. *Sol. Phys.* 293:115. doi: 10.1007/s11207-018-1333-2
- Sittler, E. C. Jr., and Guhathakurta, M. (1999). Semiempirical two-dimensional magnetohydrodynamic model of the solar corona and interplanetary medium. *Astrophys. J.* 523, 812–826. doi: 10.1086/307742
- Stanislavsky, A. A., Konovalenko, A. A., Abranin, E. P., Dorovskyy, V. V., Lecacheux, A., Rucker, H. O., et al. (2018). Revisiting the frequency drift rates of decameter type III solar bursts observed in July - August 2002. *Sol. Phys.* 293:152. doi: 10.1007/s11207-018-1374-6
- Stappers, B. W., Hessels, J. W. T., Alexov, A., Anderson, K., Coenen, T., Hassall, T., et al. (2011). Observing pulsars and fast transients with LOFAR. *Astron. Astrophys.* 530:A80. doi: 10.1051/0004-6361/201116681
- Steinberg, J. L., Aubier-Giraud, M., Leblanc, Y., and Boisshot, A. (1971). Coronal scattering, absorption and refraction of solar radiobursts. *Astron. Astrophys.* 10:362.
- Sturrock, P. A. (1964). Type III solar radio bursts. *NASA Spcl Publ.* 50:357.
- Sundkvist, D. J., Saint-Hilaire, P., Bain, H. M., Bale, S. D., Bonnell, J. W., Hurford, G. J., et al. (2016). “CURIE: cubesat radio interferometry experiment,” in *AGU Fall Meeting Abstracts*.
- Suzuki, S., and Dulk, G. A. (1985). *Bursts of Type III and Type V*. Cambridge University Press.
- Swarup, G., Ananthkrishnan, S., Kapahi, V. K., Rao, A. P., Subrahmanya, C. R., and Kulkarni, V. K. (1991). The giant metre-wave radio telescope. *Curr. Sci.* 60:95.
- Takakura, T., and Shibahashi, H. (1976). Dynamics of a cloud of fast electrons travelling through the plasma. *Sol. Phys.* 46, 323–346. doi: 10.1007/BF00149860
- Takakura, T., and Yousef, S. (1975). Type IIIb radio bursts - 80 MHz source position and theoretical model. *Sol. Phys.* 40, 421–438. doi: 10.1007/BF00162389
- Tan, B., Mészárosová, H., Karlický, M., Huang, G., and Tan, C. (2016). Microwave type III pair bursts in solar flares. *Astrophys. J.* 819:42. doi: 10.3847/0004-637X/819/1/42
- Tan, B.-L., Karlický, M., Mészárosová, H., and Huang, G.-L. (2016b). Diagnosing physical conditions near the flare energy-release sites from

- observations of solar microwave type III bursts. *Res. Astron. Astrophys.* 16:82. doi: 10.1088/1674-4527/16/5/082
- Tan, B.-L., Karlický, M., Mészárosová, H., Kashapova, L., Huang, J., Yan, Y., et al. (2016a). Diagnosing the source region of a solar burst on 26 September 2011 by using microwave type-III pairs. *Sol. Phys.* 291, 2407–2418. doi: 10.1007/s11207-016-0986-y
- Thejappa, G., and MacDowall, R. J. (2008). Effects of scattering on radio emission from the quiet sun at low frequencies. *Astrophys. J.* 676, 1338–1345. doi: 10.1086/528835
- Thurgoood, J. O., and Tsiklauri, D. (2015). Self-consistent particle-in-cell simulations of fundamental and harmonic plasma radio emission mechanisms. *Astron. Astrophys.* 584:A83. doi: 10.1051/0004-6361/201527079
- Tigik, S. F., Ziebell, L. F., Yoon, P. H., and Kontar, E. P. (2016). Two-dimensional time evolution of beam-plasma instability in the presence of binary collisions. *Astron. Astrophys.* 586:A19. doi: 10.1051/0004-6361/201527271
- Trottet, G., Pick, M., House, L., Illing, R., Sawyer, C., and Wagner, W. (1982). An association between coronal structures and type III burst sources. *Astron. Astrophys.* 111, 306–311.
- Tun Beltran, S. D., Cutchin, S., and White, S. (2015). A new look at type-III bursts and their use as coronal diagnostics. *Sol. Phys.* 290, 2423–2437. doi: 10.1007/s11207-015-0760-6
- van Haarem, M. P., Wise, M. W., Gunst, A. W., Heald, G., McKean, J. P., Hessels, J. W. T., et al. (2013). LOFAR: The Low-Frequency ARray. *Astron. Astrophys.* 556:A2. doi: 10.1051/0004-6361/201220873
- Vidojevic, S., Zaslavsky, A., Maksimovic, M., Atanackovic, O., Hoang, S., and Drazic, M. (2012). Statistical analysis of Langmuir waves associated with type III radio bursts. *Publ. Astron. Soc. Rudjer Boskovic* 11, 343–349.
- Volokitin, A. S., and Krafft, C. (2018). Electromagnetic wave emissions from a turbulent plasma with density fluctuations. *Astrophys. J.* 868:104. doi: 10.3847/1538-4357/aae7cc
- Voshchepynets, A., and Krasnoselskikh, V. (2015). Probabilistic model of beam-plasma interaction in randomly inhomogeneous solar wind. *J. Geophys. Res.* 120:10. doi: 10.1002/2015JA021705
- Voshchepynets, A., Krasnoselskikh, V., Artemyev, A., and Volokitin, A. (2015). Probabilistic model of beam-plasma interaction in randomly inhomogeneous plasma. *Astrophys. J.*, 807:38. doi: 10.1088/0004-637X/807/1/38
- Voshchepynets, A., Volokitin, A., Krasnoselskikh, V., and Krafft, C. (2017). Statistics of electric fields amplitudes in Langmuir turbulence: a numerical simulation study. *J. Geophys. Res.* 122, 3915–3934. doi: 10.1002/2017JA023898
- Wild, J. P., Sheridan, K. V., and Neylan, A. A. (1959). An investigation of the speed of the solar disturbances responsible for Type III radio bursts. *Austral. J. Phys.* 12:369. doi: 10.1071/PH590369
- Yan, Y., Chen, L., and Yu, S. (2016). “First radio burst imaging observation from Mingantu Ultrawide Spectral Radioheliograph,” in *Solar and Stellar Flares and their Effects on Planets*, eds A. G. Kosovichev, S. L. Hawley, and P. Heinzel (Cambridge University Press), 427–435. doi: 10.1017/S174392131600051X
- Yan, Y., Zhang, J., Wang, W., Liu, F., Chen, Z., and Ji, G. (2009). The Chinese spectral radioheliograph-CSRH. *Earth Moon Planets* 104, 97–100. doi: 10.1007/s11038-008-9254-y
- Zaitsev, V. V., Mityakov, N. A., and Rapoport, V. O. (1972). A dynamic theory of type III solar radio bursts. *Sol. Phys.* 24, 444–456. doi: 10.1007/BF00153387
- Zaslavsky, A., Volokitin, A. S., Krasnoselskikh, V. V., Maksimovic, M., and Bale, S. D. (2010). Spatial localization of Langmuir waves generated from an electron beam propagating in an inhomogeneous plasma: applications to the solar wind. *J. Geophys. Res.* 115:A08103. doi: 10.1029/2009JA014996
- Zhang, P., Yu, S., Kontar, E. P., and Wang, C. (2019). On the source position and duration of a solar type III radio burst observed by LOFAR. *Astrophys. J.* 885:140. doi: 10.3847/1538-4357/ab458f
- Zhang, P. J., Wang, C. B., and Ye, L. (2018). A type III radio burst automatic analysis system and statistic results for a half solar cycle with Nançay Decameter Array data. *Astron. Astrophys.* 618:A165. doi: 10.1051/0004-6361/201833260
- Zharkova, V. V., Arzner, K., Benz, A. O., Browning, P., Dauphin, C., Emslie, A. G., et al. (2011). Recent advances in understanding particle acceleration processes in solar flares. *Space Sci. Rev.* 159, 357–420. doi: 10.1007/s11214-011-9803-y
- Zheleznyakov, V. V., and Zaitsev, V. V. (1970). Contribution to the theory of type III solar radio bursts. I. *Soviet Ast.* 14:47.
- Ziebell, L. F., Petruzzellis, L. T., Yoon, P. H., Gaelzer, R., and Pavan, J. (2016). Plasma emission by counter-streaming electron beams. *Astrophys. J.* 818:61. doi: 10.3847/0004-637X/818/1/61
- Ziebell, L. F., Yoon, P. H., Gaelzer, R., and Pavan, J. (2014). Plasma emission by weak turbulence processes. *Astrophys. J. Lett.* 795:L32. doi: 10.1088/2041-8205/795/2/L32
- Ziebell, L. F., Yoon, P. H., Petruzzellis, L. T., Gaelzer, R., and Pavan, J. (2015). Plasma emission by nonlinear electromagnetic processes. *Astrophys. J.* 806:237. doi: 10.1088/0004-637X/806/2/237
- Zucca, P., Carley, E. P., Bloomfield, D. S., and Gallagher, P. T. (2014). The formation heights of coronal shocks from 2D density and Alfvén speed maps. *Astron. Astrophys.* 564:A47. doi: 10.1051/0004-6361/201322650

**Conflict of Interest:** The author declares that the research was conducted in the absence of any commercial or financial relationships that could be construed as a potential conflict of interest.

Copyright © 2020 Reid. This is an open-access article distributed under the terms of the Creative Commons Attribution License (CC BY). The use, distribution or reproduction in other forums is permitted, provided the original author(s) and the copyright owner(s) are credited and that the original publication in this journal is cited, in accordance with accepted academic practice. No use, distribution or reproduction is permitted which does not comply with these terms.